HU ISSN 1785-6892 in print
HU ISSN 2064-7522 online

DESIGN OF MACHINES AND STRUCTURES

A Publication of the University of Miskolc

Volume 5, Number 1 (2015)

Miskolc University Press
2015

HU ISSN 1785-6892 in print
HU ISSN 2064-7522 online

DESIGN OF MACHINES AND STRUCTURES

A Publication of the University of Miskolc

Volume 5, Number 1 (2015)

Miskolc University Press
2015

EDITORIAL BOARD

CONTENTS

Birta, Tamás–Herbst, Dániel–Kiss, Gábor–Kkivihalme, Krista–Kublik, Beáta–Mezei, Miklós–Oinonen, Kaisa–Parkkonen, Paavo: Morphy the Multifunctional Cordless Garden Tool-product Design Project 5

Bogomolov, Dmitry–Poroshin, Valery–Nizhnik, Valentin: Flow and Heat Flux Behaviour in Thin 2D Channel with Rough Moving Walls 15

Cermak, Roman: Design of Electromagnetic Damper Prototype for Automotive Applications 25

Hegedűs, György: Manufacturing Parameters Determination on Ball Nut Grinding 33

Kurdyuk, Vitaliy–Volskaya, Natalya: FEM Modelling of Contact Interaction Between Wheel and Supporting 39

Mazinova, Ivana: Designers and Sustainability 47

Tóth, Dániel–Szilágyi, Attila–Takács, György: Overview of Analysis Methods of Rolling Element Bearings 53

Design of Machines and Structures, Vol. 5, No. 1 (2015) pp. 5–14.

MORPHY THE MULTIFUNCTIONAL CORDLESS GARDEN TOOL – PRODUCT DESIGN PROJECT

TAMÁS BIRTA–DÁNIEL HERBST–GÁBOR KISS–
KRISTA KIVIHALME–BEÁTA KUBLIK–MIKLÓS MEZEI–
KAISA OINONEN–PAAVO PARKKONEN

University of Miskolc, Institute of Machine and Product Design
3515, Miskolc-Egyetemváros, Hungary
JAMK University of Applied Sciences
PO BOX 207, FI-40101 Jyväskylä, Finland
tamas.birta@gmail.com

Abstract: This paper is about designing a garden hand tool that means a full product design from the market research to the shape and part design. Main guidelines of the international product development project were given by Robert Bosch Power Tool Ltd. Universities of the contribution pointed on the main milestones and deadline. We assess market requirements and user needs. Our group has found possible field of improvements that can be competitive with current products and even completely new.

Keywords: *multifunctional product, product design, cordless, battery, garden tool, market*

1. Introduction

The international product development project was contributed in cooperation between the University of Miskolc, Hungary and the JAMK University of Applied Sciences, Finland. The process of the project was supported by both Finnish and Hungarian supervisors and also by the representative of Bosch. From different fields of engineering studies the students worked in a real life case for the multinational company. There were two student groups working separately on the same task. The subject of the project was about creating a cordless gardening tool with at least three functions.

The name of the tool is Morphy that comes from the Latin word: metamorphosis. It supposes to mean what our designed tool is capable of. Morphy is a lawn and garden tool, multipurpose and battery operated. It is a revolutionary cordless garden tool in its area. What people need is to make various garden tasks easier and entertain with additional technologies like smart applications, achievement system, capability of smart glasses and revolutionary design with changeable housing colour. We truly believe that gardening tasks can be fun and could mean so much more than something to get over it.

We would like to connect an ordinary multifunctional product with the latest technologies. Create your own tool, put the attachment and battery on and the fun can start right away!

2. Market research

To fulfil all the requirements from different sides, a market research had to be done; users' need had to be collected. We also had to know what users still do not know. It gives an advantage if we can come up with something new, so we need to know their environment perfectly.

The real field of competition lies in the multifunctional tools within the gardening area. Fast development of cordless technologies was the start point of innovation in the lawn and garden area. Nowadays our technologies make it possible to have effective battery operated tools, which can make our work easier. Multifunctional and compact tools are becoming more and more popular these days since the users would like their tools to consume less space and want to do as much job as they can with one device.

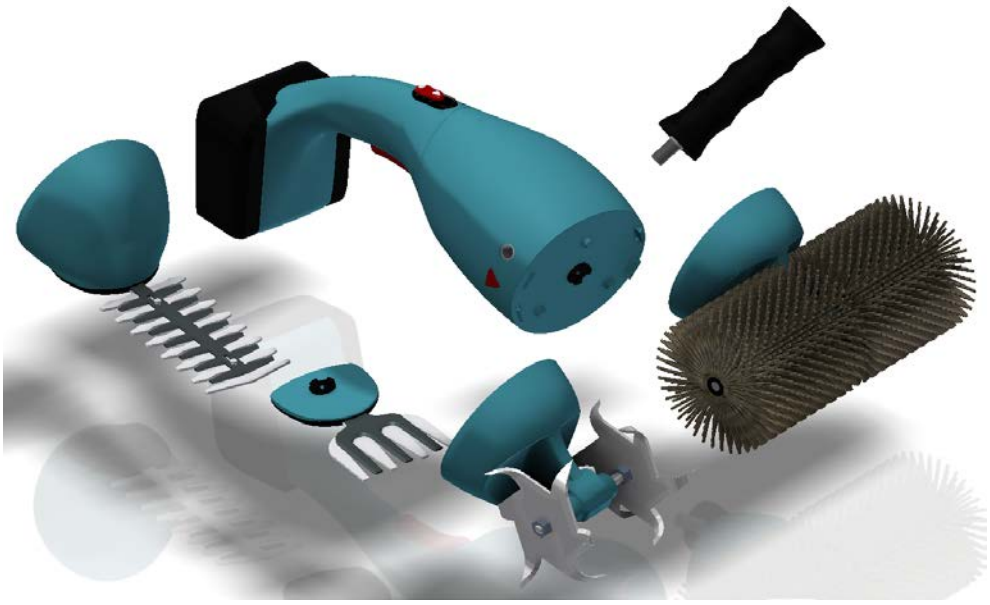

Figure 1. Morphy with its attachments

According to the online market research and gardening related forums we collected user feedbacks of the cordless gardening devices. The most annoying features are the lack of power and the short working time. The four things that users appreciate are easy handling, light weight, easily attachable battery and that the tools can be easily switched. To find out the competitive products for the concept Morphy, some research had to be done. Morphy was compared to the most similar tools available on the markets like TEHO, Bosch and Chameleon.

Our product emphasizes the things users really need. In the following there the initial concept and key messages for the user are listed.

Table 1

Key messages to user

Performance	**Ergonomics**	**User benefits**
Charging time Speed Battery capacity	Form of handle Accessibility of operating elements Balance of the tool	Light Compact Powerful Simple to use No memory effect on battery

There were also requirements from the side of Bosch but these were related somehow to compete with other market products. While focusing on the needs and requirements of the users, the principal's needs had to be kept in mind. The concept of a multifunctional cordless tool pointed the guidelines (battery size, operation time, weight).

Principal is an economic- actor, who choose, pays and use the product documentation. The most important element of user centred quality is buyer's satisfaction of the product. Because user buys the product, he/she wants to get value for his/her money.

3. Creating concepts

Morphy was created by using many alternative methods. The goal was to create something new, there needed to prepare a market analysis. This way the risk of creating something already existing is minimized.

Brainstorming was used during the whole project in different situations. The main brainstorming sessions took place already at the beginning of the project. Using this method helped us first to find of our goal and then later to generate concept in every possible subject. From the ideas some were chosen and some were left behind.

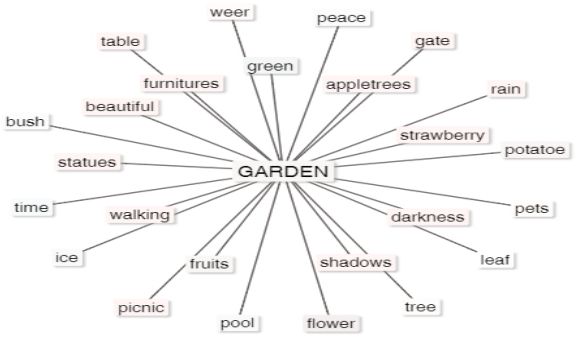

Figure 2. Brainstorming about the word "garden"

The manifestation of the developed concept is Morphy. Among the countless ideas rose up this garden tool that is based on modular principle. The name of the product can be variable depending on what users want and how marketing can touch them. If the shape of the product can be compared with a well-known thing, it is often useful to use it as an advantage. In our case Morphy is more or less shaped like a dolphin. Due to its interchangeable components, Morphy offers great flexibility for the users. It is adaptable for the particular job and for the user needs.

The research phase is followed by the feature-based conceptual design. Based on the tool's main and sub-functions a list and physical assignment has been made. The preliminary design of the building blocks was constructed here. The created solution was selected from the best variants with Copeland procedure that is based on a positive criterion consisting system of criteria. The evaluation criteria are presented in the following:

- Simplicity and Cost: It contains small number of parts and it is easy to assemble. How much does it cost to the manufacturer to make the tool? If something is simple it is not expensive so much.
- Innovation: The technical innovation that catches the user.
- Energy usage: How efficiently the tool use the energy stored in the battery?

– Handling: How obvious the interface is and how clear the tool's shape hints to the right usage.
– Comfort: In which conditions the user uses the tool and how clear and conspicuous the feedback is from the tool.

The adequate level of comfort of users is provided by ergonomic considerations. The human-centred design helps prevent the loss of comfort for the users, in case of a longer period of usage.

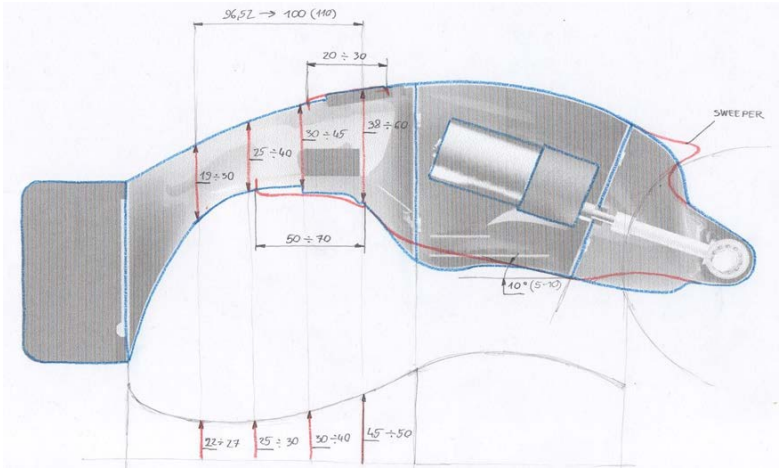

Figure 3. Sketch of the back grip and body

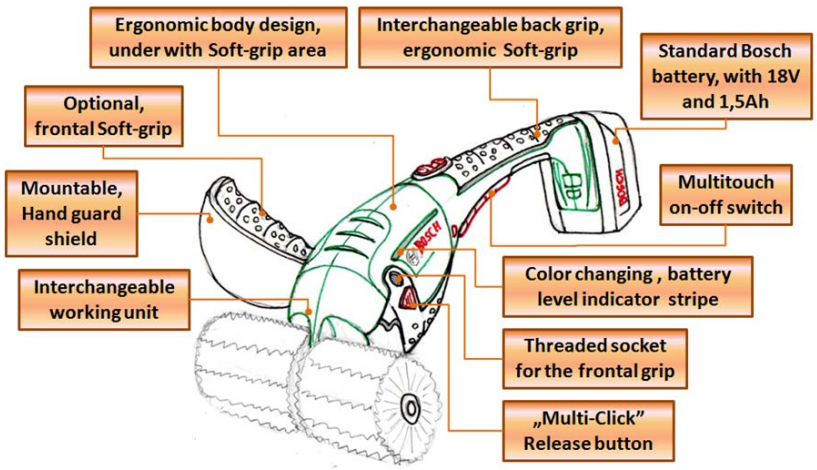

Figure 4. Charming features on the garden tool

Anthropometric dimensions for the ergonomic body design came from measurements, and professional literature research (EN 14866). Main target was the back grip, because this subpart must be comfortable with the switches.

The design of the frontal grip takes into account the average size of the fingers and their distance from each other. There are threaded holders on both sides of the main unit to

support the right and left-handed usage. To ensure the safety of the users, the frontal grip can be provided with hand guard cover.

4. Solutions

Based on the functional list of Morphy the main components can be determined. The body shape, the shape of housing is based on ergonomic considerations, but it takes into account the function fulfilment of the functional components.

After long deliberation, we have chosen the main attachments, which are the hedge trimmer, sweeper and cultivator. Also some promising attachment ideas have been predesigned like weed puller multi tool and weed sweeper.

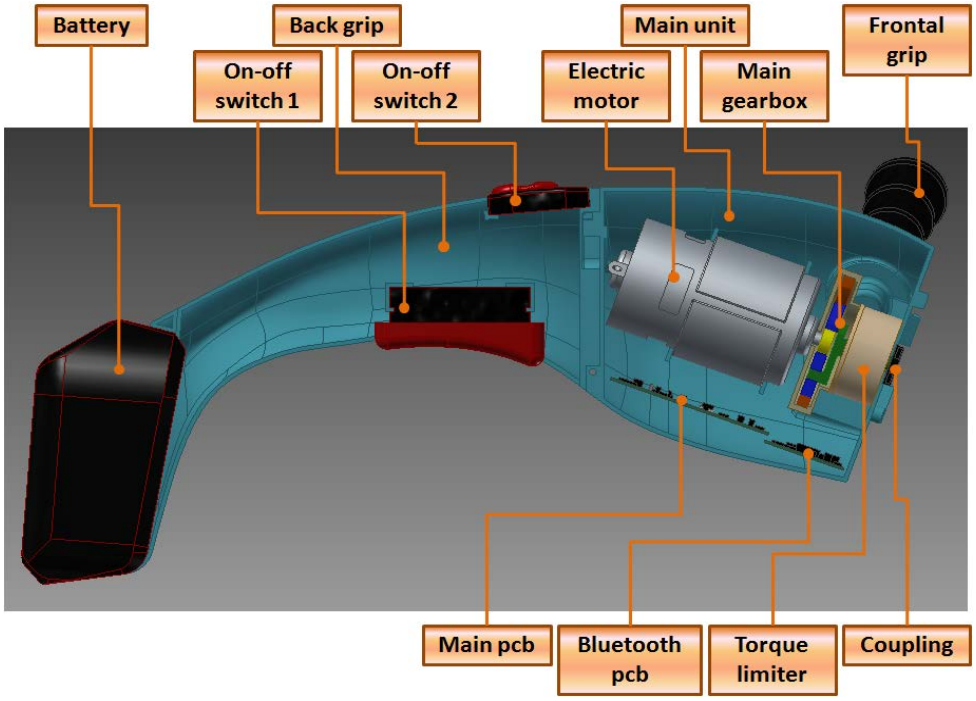

Figure 5. Preliminary internal structure of Morphy

Engineering calculations are based on the functional analysis of the internal structure of Morphy. We have chosen one solution for the structure and tried to estimate the related main data. These were the power supplied by the battery, and the torque what we need for the approximated function. Going through the design process, we have got the rough components with their size (motor, couplings, planetary gears, shafts).

Among the possible attachments, the hedge trimmer attachment has the highest rotation speed. The output rotation speed have to be around 3000 rpm, in this case the further transmission ratio reduction can be easily implemented.

For torque limiter we use a common mechanism. It has 4 main parts. It has a cylinder to carry balls, balls, a shaped counterpart and a spring. A spring squeezes the two cylinder parts. If the torque is too big the two parts can rotate on each other because of the balls.

4.1. Sweeper

Sweeper is the tool of health and cleanness. It is already alone a multi-purpose tool to clean the greenhouse, floor, tables, shelves, plant pots and all of your garden tools. It can help not only in the garden, but also with cleaning anything from snow and from dust. With the pole cart extension tool of Bosch, high places can be reached. It can be equipped by several types of brushes, stiffness and size of the threads can change. It is the perfect solution that fits every hand and helps for every age to make cleaning more fun.

Calculation of the attachments was made based on the power need of the working main function. The power consumption comes from the needed rotational moment of the tool's shaft. It was calculated from the force needed to push away the specified amount of material.

Planetary gear can be used in the sweeper attachments to reduce the rotation speed near to 1000 rpm. It was necessary to gain as much torque as possible for sweeping. The insight components of the sweeper are presented in the figure below.

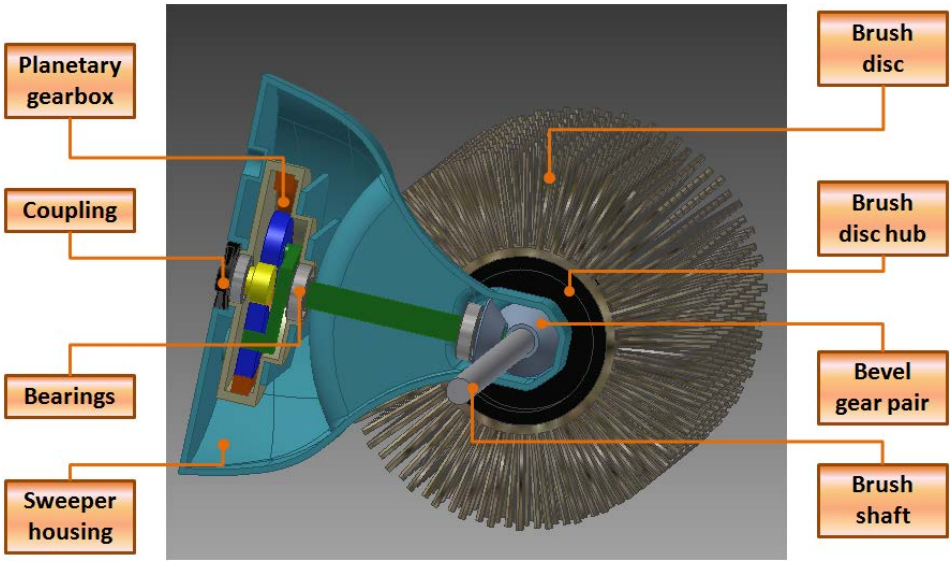

Figure 6. Section view of the sweeper attachment

Summarized data for the sweeper:
Sweeps dust/soil/dirt/sand from narrow places
Max effective height of swept material: 50 mm
Rotation speed: ~ 1000 rpm
Dimension: ⌀80x165 mm
Estimate continuous operational time in normal use: ~ 40 min
Power need in normal use 42 W.

4.2. Cultivator

A small one-hand cultivator tool is another attachment for Morphy. Cultivator tool is designed to loosen the ground in small vegetable gardens and greenhouses. It digs, blends soil with fertilizer. Cultivator has bended steel blade to do perfect work.

For the cultivator it is also a good solution to use a planetary gear for speed reduction. In this case it transmits the 3000 rpm rotation speed (which comes from Morphy) to nearly 100 rpm. It means nearly 30 transmission ratio, which can only be carried out in two stages in small size. The other side of the cultivator tool's gearbox is a simple bevel gear pair, with 1 to 1 transmission ratio, to turn 90 degrees of the direction of rotation, as in the case of the sweeper tool.

Our calculations gave only a rough result. It is based on the power of rotating an amount of soil. The real value varies a lot depending on pushing force and friction.

This idea uses the same size components and parts as sweeper for modularity. Difference between sweeper and cultivator design is that the cultivator has stronger blade shaft and size of shaft bearings. Cultivator has different rotating speed so different gearbox is also needed.

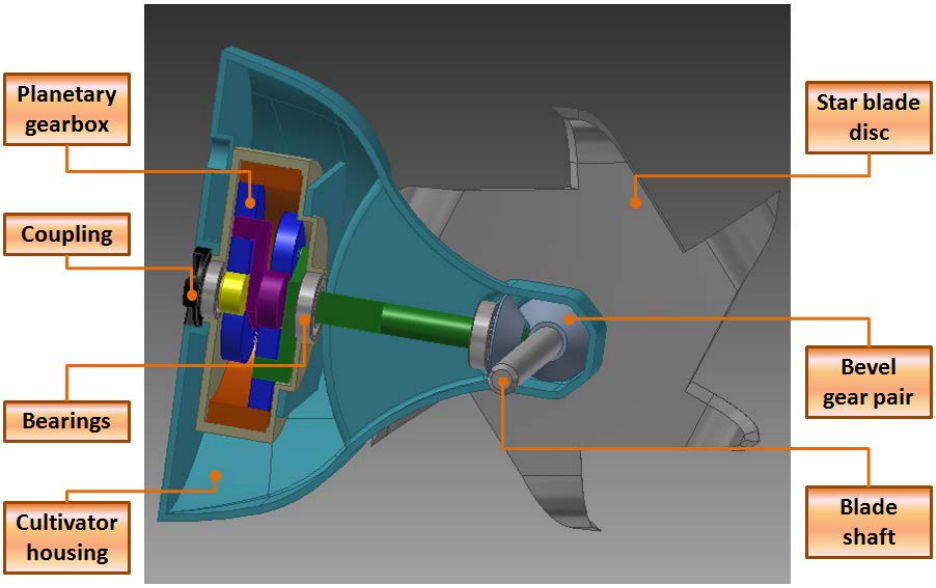

Figure 7. Final design of the inside of the cultivating tool

4.3. Weed puller rotary tool with spiral shaped blades

Weed puller multi-tool is a multifunctional easy-to-attach extension. The main concept of the spiral shaped bladed attachment comes from the paint mixer and the rotary weed puller what are used normally with drilling machines, or battery operated drill-drivers. The auger type tools with half to two pitch can be used for hole digging and soil, humus mixing. With a special geometry blade, this is capable of doing all those jobs. The blade spiral angle is increased, and beside the rotating shaft is undercut. This geometry allows the tool to be able

to dig holes and also weed is entangled in the rotating blades. This tool could stand alone, as it can be sold even with other Bosch products as an extension.

4.4. Weed sweeper

Weed sweeper is a weed cutting attachment. This is a special purpose tool to cut grass and weeds from narrow places. This high speed tool with hard brushes cut the weeds out like a string grass trimmer, but this tool rotates in vertical plane. The structure of this attachment is related to the design of the sweeper.

4.5. Bush shaper

Bush shaper tools are the ordinary function of the present Bosch products. The basics for these grass trimming and hedge cutting function came from the product Isio. In our concept, it was a basic function what should be implemented in a multi-functional garden tool.

5. Smart solutions

Customers always would like to feel better from their new products, and their expectations are growing year-to-year. Nowadays the biggest trend is the smart gadgets. Other brands try to make everything smart, and this will cause the “smartness” to become a future basic expectation.

Our idea for this problem is the Personal Gardening Assistant (PGA). This application will run on the basic operation systems, which will be compatible with smart phones, glasses and watches. The main function will be the connectivity. Users will be able to connect their gadgets to garden tools and with this they will easily get information about the tool furthermore they will have the option to control it. Smart solutions will open a new field on the market.

5.1. Virtual reality

Virtual reality can be a huge hit in a few years, and that will be a good idea to think about the smart gadget options. In the future users will be able to be more professional with the Bosch applications.

Figure 8. Working area detection via specified prerequisite

It will also give advice about the most convenient tool, and if they do not have it also recommend a nearby reseller.

Working area detection can be also a huge hit in the future, because the user will easily calculate how much time it will cost to do the work.

5.2. Experience based levelling

Nowadays other trends are the micro transaction games, which are about that people will always want to get to the other level, and compete with other people and get their well-deserved prizes. These games give the idea to make this application to more game-like. But every game need a competitive system and this is the experience base levelling. If people buy Bosch products they will get experience, and they will level up and also gain sale points.

Basically we want to use the human nature. Everybody wants to be better than the others. This is why we need experience point, because with these the user will level up, and the level is where they can compete with each other. Sale point is very different from the last two. The user can consume them to get different prizes depends on their level. For example at early level they can get only some euro discounts, but later they will get bigger prizes; which means percentage discounts. This system makes the user more loyal to Bosch. It will be like a point card system.

5.3. Positive feedback

Every game has to give positive feedback to the users. The absolute basic components can be the achievements. In this application the achievements will be the most important experience and discount source. For example Bosch can make competitions for local communities in a seasonal holiday topic, where the competitors will get an achievement.

5.4. Tie-in sales

Tie-in sales will be the main profit source of the application. Achievements will give a discount for another Bosch family product. For example with a gardening tool they will get a Bosch Home discount. The user will go to the reseller store and see a lot of brands, but they will not care about them, because only one company give them a discount already, and this can be enough for an average user. This will also increase the loyalty for the Bosch products.

The previously detailed game-like systems works well when connected. They bring the users closer to Bosch and closer to their hobbies.

6. Failure mode and effects analysis

Failure modes and effects analysis (FMEA) is a step-by-step approach for identifying all possible failures in a design, manufacturing or assembly process, or a product or service.

The first stage of FMEA was made for the motor, gearbox and housing.

Once actions have been completed, re-scoring the occurrence and detection is necessary. In most cases there is no need to change the severity score unless the customer decides this is not an important issue.

7. Purchasing

In this project, the purchasing was a major part for gathering information about the suppliers and marketing prices.

At low production rate the injection moulding price is significant so this is where the company can cut expenses and increase the profit. But at higher rate, the battery, charger

and dc motor can be the components where the company can make an extra profit if they can manage to cut the cost.

8. Summary

Using the full scale of product design tools like market research, risk analysis, FMEA, design book, brainstorming, solution evaluation methods… etc. showed the future way of garden tool improvements. We have made a preliminary model of an ergonomic battery operated multifunctional tool for garden works.

9. Acknowledgement

The whole project team feels proud and privileged to work with each other and get to know new ways of thinking and working. Warm thank for Dr. József Kakuk for enabling this opportunity to work with Bosch. We are also grateful for our supervisors from Hungary, Vadászné Dr. Bognár Gabriella, Kelemen László and Dr. Szabó J. Ferenc, as also for our Finnish supervisors, Jorma Matilainen, Petri Luosma and Anneli Kakko.

Design of Machines and Structures, Vol. 5, No. 1 (2015) pp. 15–24.

FLOW AND HEAT FLUX BEHAVIOUR IN THIN 2D CHANNEL WITH ROUGH MOVING WALLS

DMITRY BOGOMOLOV–VALERY POROSHIN–VALENTIN NIZHNIK

Moscow State Industrial University
115280, Avtozavodskaya st. 16, Moscow, Russia
bogom-ov@mail.ru,vporoshin@mail.ru, valngnk@yandex.ru

Abstract: Paper describes the investigation of flow and heat flux in thin channel with rough moving walls in the 2D approach. The effect of the real measured roughness profiles upon Nusselt-number in comparison with smooth wall channel is shown. Both static and dynamic flow components were investigated.

Keywords: *thin channel, surface roughness, fluid flow, heat flux, moving wall*

1. Introduction

Study of the fluid flow and heat flux in thin channels of technological devices is one of the main problems of modern applied mechanics. Practical aspects of the problem are referred to the heat flux intensification in compact heat exchangers, heat flux study in moving parts of pumps and engines and so on. Behaviour of the flow and heat flux in the thin channel differs from the same processes in large size channels. Due to the small gap size, surface roughness becomes one of the main factors, having great impact on the resulted leakage and heat-exchange rate in the channel. One of the common ways to stimulate heat-exchange in large channels and pipes (especially for turbulent flow) is to produce some regular surface texture on its' walls. In the small channel the surface texture influence should be even more clear.

In authors' earlier work [1] the mathematical model of heat flux in the thin channels with rough immovable walls was proposed. Present work is an attempt for extending our researches over the heat flux in channels with rough moving walls. Such model allows to analyse the roughness effect upon the static and dynamic components of flow and heat flux in the thin channel.

2. Calculation model

The geometry model of the thin channel with moving walls formed by two rough surfaces h_1, h_2 is presented in Figure 1. The gap between two rough surfaces (H) is taken as the distance between their mean lines. Upper and lower walls has coordinates $H_1(x) = H + h_1(x)$ and $H_2(x) = H + h_2(x)$. The current gap in the channel is calculated as $h_T(x) = H + h_1(x) + h_2(x)$. The upper wall slides in parallel direction to the lower with constant U speed.

Measured profiles of the real industrial surfaces or simulated roughness profiles with desirable features can be used as a surface geometry. Both profiles are always specified on regular grid with Δx step. Calculation step in x direction is considered as some fraction of the profile grid step $\Delta x = k\delta x$ (where k is an integer value). Calculation step in y direction δy is also considered regular comparable to δx.

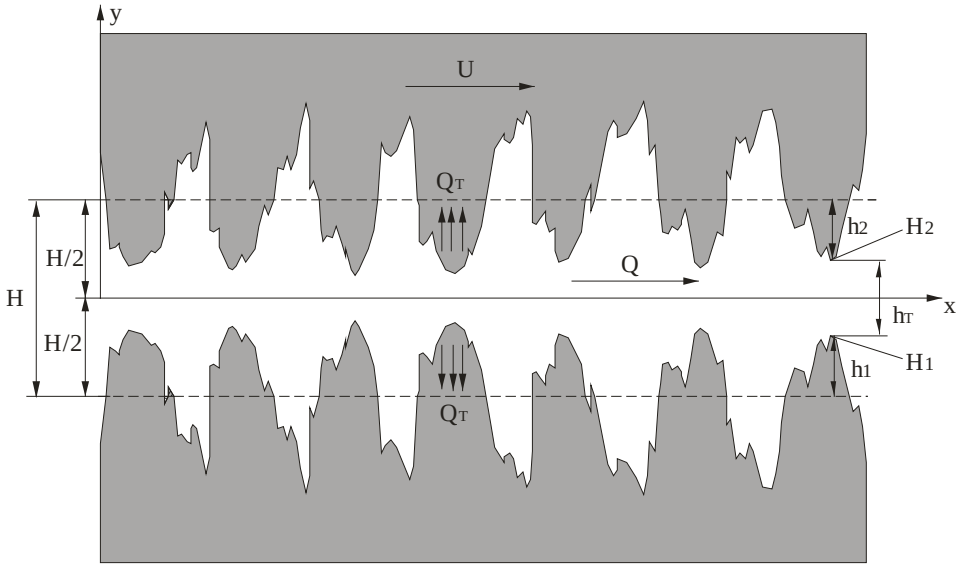

Figure 1. Geometry model of the thin channel with rough moving walls

To model the flow in the described thin channel the lubrication flow model was proposed. It is based on the common Reynolds equation (3D case):

$$\frac{\partial}{\partial x}\left(h_T^3\frac{\partial p}{\partial x}\right)+\frac{\partial}{\partial y}\left(h_T^3\frac{\partial p}{\partial y}\right)=6\mu U\frac{\partial h_T}{\partial x},\quad v_z=0, \tag{1}$$

$$v_x=\frac{1}{2\mu}\frac{\partial p}{\partial x}z\left(z-h_T\right)+U\left(1-\frac{z}{h_T}\right),\quad v_y=\frac{1}{2\mu}\frac{\partial p}{\partial y}z\left(z-h_T\right),$$

where p is the flow pressure, v is the local flow velocity, μ is the dynamic viscosity. For the 2D case Reynolds equation is significantly simplified and can be solved analytically, as shown in [2].

$$p(x)=p_{in}+6\mu U\int_0^x\frac{d\xi}{h_T^2(\xi)}+\frac{p_{out}-p_{in}-6\mu U\int_0^L\frac{d\xi}{h_T^2(\xi)}}{\int_0^L\frac{d\xi}{h_T^3(\xi)}}\int_0^x\frac{d\xi}{h_T^3(\xi)},$$

$$\frac{\partial p}{\partial x}=\frac{6\mu U}{h_T^2(x)}+\frac{p_{out}-p_{in}-6\mu U\int_0^L\frac{d\xi}{h_T^2(\xi)}}{h_T^3(x)\int_0^L\frac{d\xi}{h_T^3(\xi)}}, \tag{2}$$

where p_{in} is the pressure at the channel inlet, p_{out} is the pressure at the channel outlet (boundary conditions).

To model the conjugated to the flow heat flux the thermal balance equation is commonly used:

$$\rho C_p \frac{dT}{dt} = \lambda \Delta(T) + \mu\Phi, \tag{3}$$

where T is the local flow temperature, ρ is the media density, C_p is the media thermal capacity, λ is the media thermal conductivity, t is the time, Φ is the dissipative function. The dissipation process is not natural for the described problem, so Φ was neglected in the proposed model.

The flow in the 2D thin channel is in general ordered in x direction, from inlet to the outlet. So $v_y = 0$ is considered from the flow equation. Supposing the process as stationary it gives:

$$\frac{dT}{dt} = v_x \frac{dT}{dx} + v_y \frac{dT}{dy} = v_x \frac{dT}{dx}. \tag{4}$$

The heat transfer in the 2D thin channel is generally ordered in y direction, from channel walls to the flow media. So d^2T/dx^2 in the Laplace operator was also neglected. The resulting heat transfer model is:

$$\rho C_p v_x \frac{dT}{dx} = \lambda \frac{d^2T}{dy^2}. \tag{5}$$

Equation (5), being the simplified approach to (3), still takes into account main process features.

Difference problem (5) was solved with known temperature T_w at the channel walls and known temperature of the flow T_{in} at the channel inlet. Under such boundary conditions the problem was solved by using the implicit finite-difference method. The stencil for that method is shown in Figure 2.

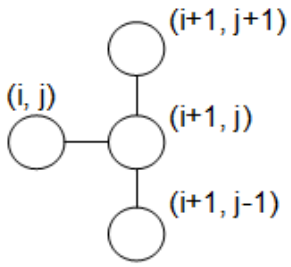

Figure 2. Implicit finite difference stencil for the thermal balance equation

According to the implicit finite difference method the temperature derivatives are substituted by the following finite differences:

$$\frac{dT}{dx} = \frac{T_{i+1,j} - T_{i,j}}{\delta x}, \quad \frac{d^2T}{dy^2} = \frac{T_{i+1,j-1} - 2T_{i+1,j} + T_{i+1,j+1}}{\delta y^2}. \tag{6}$$

So, the (5) equation is substituted by the following finite difference equation:

$$\rho C_p \left[v_x\right]_{i,j} \frac{T_{i+1,j} - T_{i,j}}{\delta x} = \lambda \frac{T_{i+1,j-1} - 2T_{i+1,j} + T_{i+1,j+1}}{\delta y^2}. \quad (7)$$

The sweep method (tridiagonal matrix algorithm) was used for the solution of (7). The scheme is always numerically stable and convergent. The scheme errors are linear in x direction and quadratic in y direction.

3. Heat flux characterisation

The operational capacity of the thin channel with rough walls was assessed by means of flow factors, and Nusselt-number. The dimensionless flow factors φ_x and Θ_x shows how decreases the leakage through the channel Q in comparison to the leakage through the equal channel with smooth walls Q*:

$$Q_x^* = \frac{BH^3(p_{out} - p_{in})}{12\mu L} + \frac{BUH}{2}. \quad (8)$$

where B is the channel thickness.

It is clear from (8) that the flow is the algebraic sum of two flow components. The first component is the static flow. It is caused by the pressure gradient at the channel inlet and outlet. The second component is the dynamic flow. It is caused by the channel wall sliding. So, different flow factors for dynamical and static flow components should be calculated.

The static flow factor φ_x should be calculated taking into account only static part of leakage and not taking into account the wall movement (U=0):

$$Q_{xs} = \frac{Bh_T(L)^3}{12\mu} \left.\frac{\partial p}{\partial x}\right|_{x=L} = \frac{B\left(p_{out} - p_{in}\right)}{12\mu \int_0^L \frac{d\xi}{h_T^3(\xi)}},$$

$$Q_{xs}^* = -\frac{BH^3(p_{out} - p_{in})}{12\mu L}, \varphi_x = Q_{xs} / Q_{xs}^*. \quad (9)$$

The dynamical flow factor Θ_x is calculated taking into account only dynamic part of leakage and not taking into account the pressure gradient on the channel inlet and outlet:

$$Q_{xd} = BU \int_0^L \frac{d\xi}{h_T^2(\xi)} \Big/ 2\int_0^L \frac{d\xi}{h_T^3(\xi)},$$

$$Q_{xd}^* = \frac{BUH}{2}, \theta_x = Q_{xd} / Q_{xd}^*. \quad (10)$$

Such method of flow factors calculation provides that both of them do not depend on particular values of wall sliding velocity U and pressure gradient, viscosity and so on. They are mostly determined by the roughness form and roughness-to-gap proportion.

The Nusselt-number is the ratio of convective and conductive heat transfer normal to the boundary. The conductive component is measured under the same conditions as the heat convection but with a stagnant flow. In our case this dimensionless shows the efficiency of the reviewed channel for managing the heat transfer by manipulating the flow pressure and wall velocity.

For the fully developed laminar flow the Nusselt-number, calculated for some cross section (x = const) is [3]:

$$Nu = \frac{\alpha D_h}{\lambda}, \tag{11}$$

where α is the convective heat transfer coefficient, D_h is the hydraulic diameter. The hydraulic diameter of the channel in section is:

$$D_h = \frac{4 A_c}{P} = \frac{4BH}{2B+2H} = \frac{2BH}{B+H}, \tag{12}$$

where A_c is the cross sectional area, P is the wetted perimeter of the cross section.

The convective heat transfer coefficient of the channel is calculated as:

$$\alpha = \frac{q}{T_w - T_m}, \tag{13}$$

where q is the normal heat flux near the walls, T_m is the representative flow temperature in the section.

The normal heat flux near the walls was calculated neglecting the roughness slopes as:

$$q = \lambda \frac{\partial T}{\partial y}. \tag{14}$$

The representative flow temperature was calculated by averaging the flow temperatures concerning the flow velocity:

$$T_m(x) = \int_{H_1(x)}^{H_2(x)} v_x(y) T(y)\, dy \Big/ \int_{H_1(x)}^{H_2(x)} v_x(y)\, dy. \tag{15}$$

The resulting Nusselt-number of the flow can be calculated by averaging the Nusselt-numbers in all the cross-sections of the channel except the developing zone near the channel inlet. The distinct static and dynamic Nusselt-numbers can be calculated for both static and dynamic case of the boundary condition.

4. Analysis

To verify the developed calculation model and computation software the channel with smooth walls was examined, which has already been studied by many authors [4]. In the stated assumptions the flow process is hydraulically developed from the beginning and flow velocity in any cross section has parabolic form. For the heat flux there is some zone near the channel inlet in which the process is developing. For the developed process the cross section of the temperature field has a clear parabolic shape. For the developing process it has a shape of flattened parabola. The results of the numerical experiments are agreed to the expected process behaviour. The resulting evolution of the heat flux in the channel with smooth walls is shown in Figure 3.

The quasy-parabolic distribution of the temperature was achieved for the inner sections of the channel (Figure 3b). The centre of the temperature distribution is shifted towards the moving wall direction. This is due to the higher velocity of the flow near the moving wall. Near the channel inlet the cross-section temperature gradually evolutes from the constant boundary condition to the quasy-parabolic form (Figure 3a).

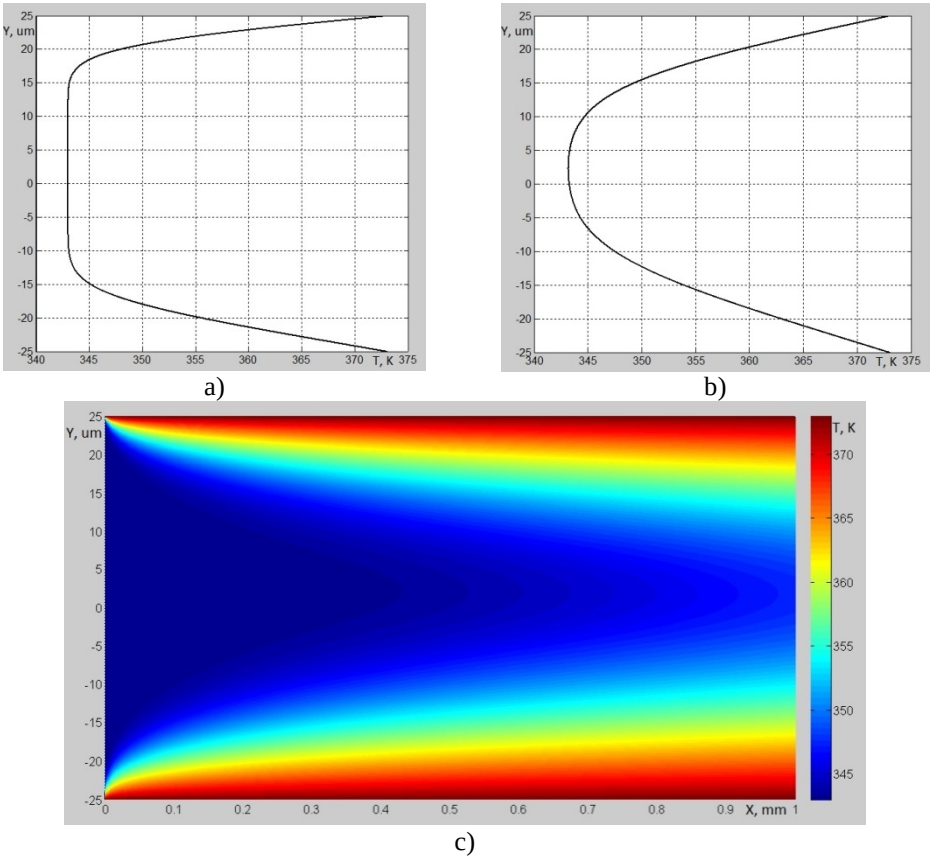

Figure 3. Flow temperature in the channel with smooth walls
a) – cross-section of flow temperature near the channel inlet, b) – cross-section of flow temperature in the middle zone, c) – flow temperature field

In complex the results achieved for the smooth wall channels allow to validate the correctness of the proposed numerical model.

Other numerical experiments were carried out for the rough wall channels. The surfaces after polishing, grinding, milling and turning were used (Figure 4). The length of the analysed channel was 0,8mm.

The experiments were carried out for H = 40μm, p_A = 10kPa, p_B = 0, U = 200m/s, T_{in} = 343K, T_w = 373K. Typical flow temperature fields for the static boundary condition is shown in Figure 5. Typical flow temperature fields for the dynamic boundary condition is shown in Figure 6.

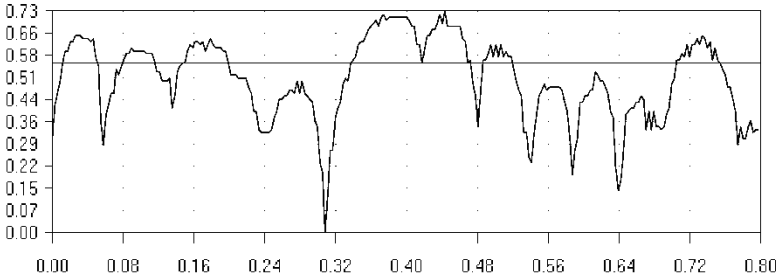

surface after polishing

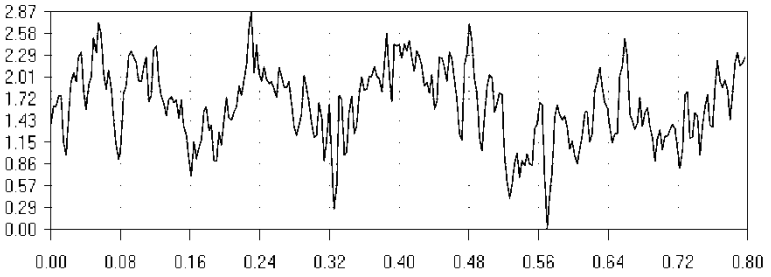

surface after grinding

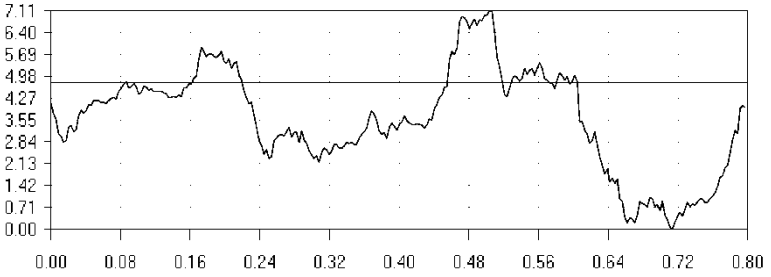

surface after milling

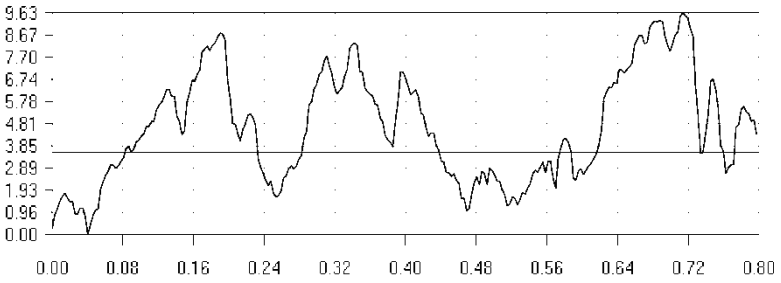

surface after turning

Figure 4. Surface roughness profiles

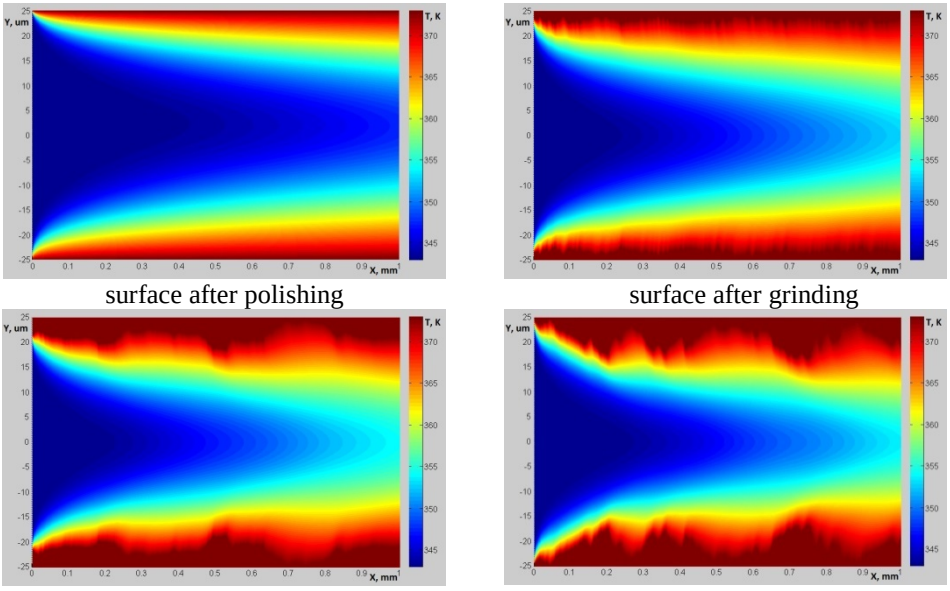

Figure 5. Flow temperature fields in channels with rough walls and static flow boundary

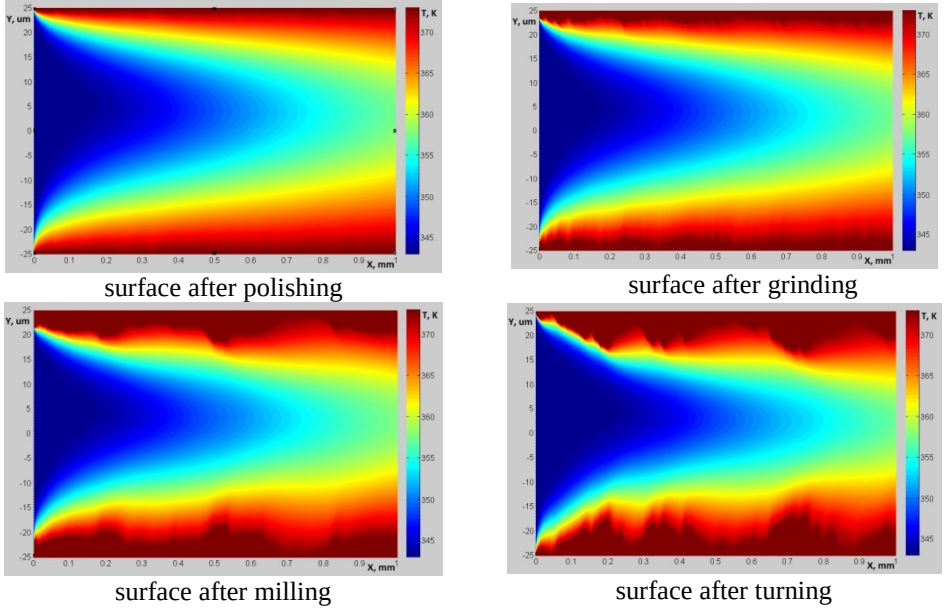

Figure 6. Flow temperature fields in channels with rough walls and dynamic flow boundary

The cross sections of the flow temperature fields are also has a quasy parabolic shape as for the smooth channel. There is also zone of the developing flow near the channel inlet. The heat flux is more intensive for the greater roughness heights.

The resulting Nusselt-number evolution for flows in channels with different surface roughness for static and dynamic boundary conditions are shown in Figure 7, 8. The results are shown as a graph of the Nusselt-number evolution while growing of the average gap from 40 to 60 um.

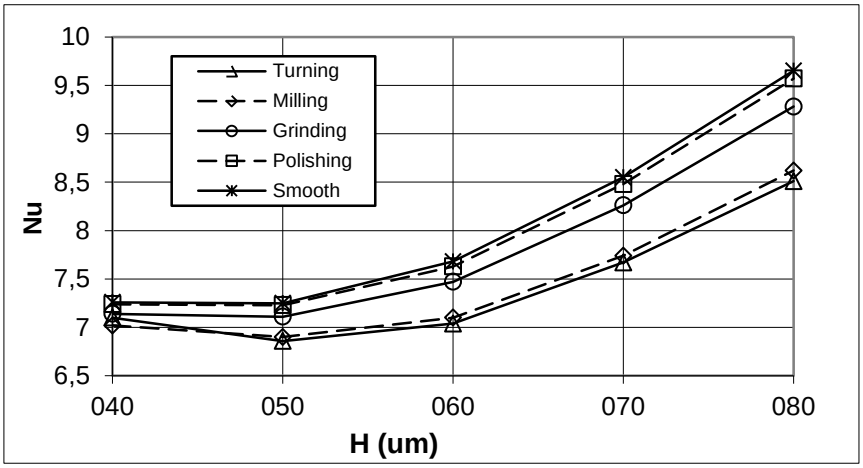

Figure 7. Evolution of Nusselt-number for static flow component

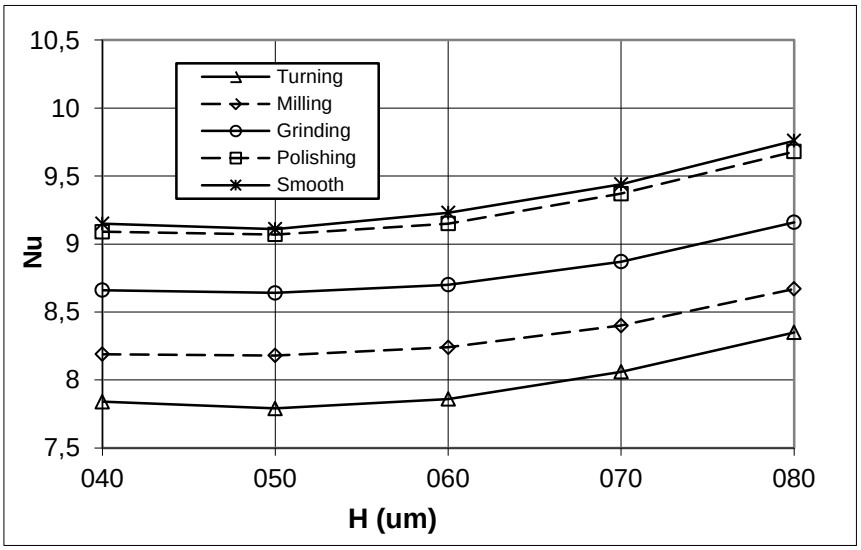

Figure 8. Evolution of Nusselt-number for dynamic flow component

Nusselt-number grows with growing average gap, because Reynolds-number of the flow also grows. It is consistent to the known theoretical assumptions and experimental data for macro-size channels.

For both static and dynamic flow components the Nusselt-numbers for the rough surfaces becomes more distinct from the smooth channel ones with growing of the average gap. But the difference in Nusselt-numbers is much lesser for the more thin channels.

For the static case the mean flow temperature is located approximately in the middle of the channel vertical section. The central flow layers are mostly affect the resulting Nusselt-number. For the dynamic case the mean flow temperature is biased in the direction of moving wall. The layers adjacent to the moving wall are much more involved into the heat flux. The Nu curves for the dynamic case are quite parallel to each other. That is an unsuspected fact that requires further detailed investigation.

5. Conclusion

Proposed mathematical model allows to forecast flow and heat flux in 2D channels with rough moving walls. It can be effective for the optimal selection of the processing methods of surfaces at the projecting stage.

Numerical experiments show that the surface roughness have a great influence upon the heat flux. For both static and dynamic flow components the Nusselt-numbers for the rough surfaces becomes more distinct from the smooth channel ones with growing of the average gap.

The research was performed with the financial support of the Ministry of Education and Science of the Russian Federation for higher education institutions within the state job service.

6. References

[1] BOGOMOLOV, D.–POROSHYN, V.–LYSENKO, V.–ONANKO, A.: Modeling of Flow and Heat Transfer in Thin 2D Channels with Rough Walls. *Advanced Engineering*, 2011, 2, 147–154.

[2] SHEJPAK, A.–POROSHIN, V.–SYROMIATNIKOVA, A.–BOGOMOLOV, D.: Roughness Influence upon the Hermeticity of Plunged Pair Using Equivalent Gap Model. *Advanced Engineering*, 2008, 2, 283–290.

[3] ROHSENOW, Warren M.–HARTNETT, James R.–CHO, Young I.: *Handbook of Heat Transfer*. MCGRAW-HILL, 1998.

[4] MILLS, A. F.: *Heat Transfer*. 2nd Ed. Prentice Hall, Upper Saddle River, New Jersey, 1999.

Design of Machines and Structures, Vol. 5, No. 1 (2015) pp. 25–32.

DESIGN OF ELECTROMAGNETIC DAMPER PROTOTYPE FOR AUTOMOTIVE APPLICATIONS

ROMAN ČERMÁK

University of West Bohemia, Department of Machine Design
30614, Plzen, Czech Republic
rcermak@kks.zcu.cz

Abstract: The paper deals with design of an electromagnetic damper prototype. An introduction to the automotive dampers is given and motivation is mentioned. Modelling of the dampers using quarter car model and full car model are described. Several design variants of the damper were studied and briefly discussed in the text. First case was a passive damper based on energy dissipation due to eddy currents created by movement of permanent magnet inside a massive copper tube. In the second case the copper tube is replaced by set of coils. It allows adjusting damper parameters, applying active and semi-active concepts and opening a possibility for energy recovery. A test facility used designed for out-of-the-vehicle testing of automotive dampers is mentioned at the end of the paper.

Keywords: *shock absorber, electromagnetic damper, energy recovery*

1. Introduction

Automotive suspension is one of the key components in nowadays cars. Proper suspension design can significantly improve vehicle behaviour and safety.

The automotive suspension on a vehicle typically has the following functions [4]:

- to isolate a car body from road disturbances in order to provide good ride quality. i.e. to reduce vibrations transmitted from the axle to the body/passenger, i.e. reduce body acceleration .
- to keep good road holding (cornering, braking, traction) – i.e. variations in normal tire loads are minimized. Since a tire roughly behaves as a spring, it can be directly related to vertical tire deflection.
- to provide good handling – i.e. minimize the roll and pitch motion.
- to support vehicle static weight – i.e. rattle space requirements are kept small.

The analysis of passive automotive suspension in literature (e.g. [1, 2, 3, 4]) shows, that there are significant trade-offs in performance between the ride quality, rattle space and tire deflection transfer functions. Improvements in one of them usually deteriorate the other two transfer functions. Therefore active and semi-active suspensions were introduced.

The fundamental difference between active and semi-active control strategy is in the form of input energy. While active suspension uses force actuator to control motion of the body (i.e. it needs enough energy to move the body with the desired velocity and acceleration), semi-active suspension system utilizes a variable damper or other dissipation component (see Figure1). Compared to active suspension, semi-active one consumes significantly less power.

Various published studies (e.g. [8, 10]) show, that energy of ap. 100–1600 W (depending on other factors) dissipates in a damper of common cars. Studies further show, that ap.10% of the dissipated energy can be recuperated.

2. Suspension modelling

A brief introduction to the suspension modelling is given in this section.

2.1. Quarter car models

Simplified models are very often used for modelling of vehicle suspension. Typical example is using of a quarter-car model for description of vertical motion of vehicle. The model is very simple and gives relevant results. For more complex study (including roll and pitch motions etc.) a half-car or a full-car model must be used.

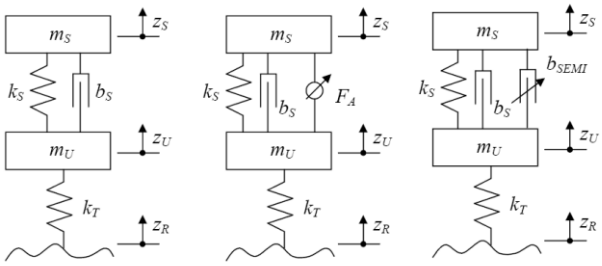

Figure 1. A quarter-car model – from left to right: passive suspension, active suspension, semi-active suspension

Equation of motion for quarter car model can be expressed in the following form [2]:

$$\begin{bmatrix} m_S & 0 \\ 0 & m_U \end{bmatrix}\begin{bmatrix} \ddot{z}_S \\ \ddot{z}_U \end{bmatrix}+\begin{bmatrix} b_S & -b_S \\ -b_S & b_S+b_T \end{bmatrix}\begin{bmatrix} \dot{z}_S \\ \dot{z}_U \end{bmatrix}+\begin{bmatrix} k_S & -k_S \\ -k_S & k_S+k_T \end{bmatrix}\begin{bmatrix} z_S \\ z_U \end{bmatrix}=\begin{bmatrix} 0 \\ k_T \end{bmatrix}z_R+\begin{bmatrix} 0 \\ b_T \end{bmatrix}\dot{z}_R+\begin{bmatrix} 1 \\ -1 \end{bmatrix}F_A$$

Detailed mathematical description of the models can be found in the literature (e.g. [1, 2, 3, 4]). For complex manoeuvre simulation the quarter car model doesn't offer enough information and an integration of the suspension model into full car model is required. The complete full car model usually includes sub models of powertrain, driveline, tires, brakes, steering etc. Development of such a complex model takes lots of effort, and it is easier to use one of the commercially available and proven solutions described in the following section.

2.2. Full vehicle models

For overall understanding of vehicle behaviour, it is useful to model the vehicle in one of available commercial software packages, which provide the user proven and quite complex models of vehicle components. Typical example of such a software package is ADAMS and it's automotive modules called ADAMS/Car. ADAMS also offers possibility of co-simulation with software like MATLAB/Simulink and with EASY5.

ADAMS/Car provides the user with an easy way how the overall car model can be build. It uses so called template based approach, i.e. each component is described in a template, which is used to generate a subsystem as a part of the full vehicle assembly.

Shock absorber properties are defined in a property file, an ASCII file with the force-velocity curve definition.

Among above mentioned the SW provide user with a number of pre-defined manoeuvres and a tool – event builder – for creating user-defined manoeuvres. The SW contains a tool Road Builder for creating a test track with various obstacles (compliant road is also available). Many various functionalities as Smart Driver, DoE and optimisation options are available in the SW.

There is an example of a road with several obstacles and a simulation results for a demo vehicle running across.

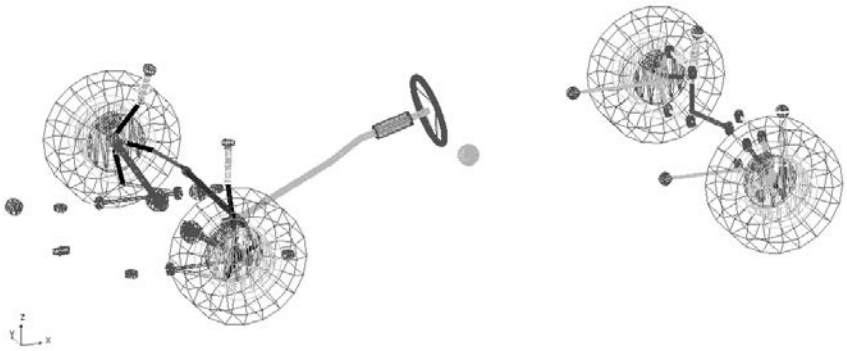

Figure 2. Graphical representation of a full vehicle model in ADAMS/Car package

Complex simulation option of the full vehicle exposed to different road conditions, driver behaviour etc., gives the users an excellent opportunity to investigate complex tasks in the virtual reality.

2.3. Electromagnetic passive damper

However using of electromagnetic shock absorber is quite rare in the commercial applications, it is very often discussed in the scientific papers. There are several principles described on the literature.

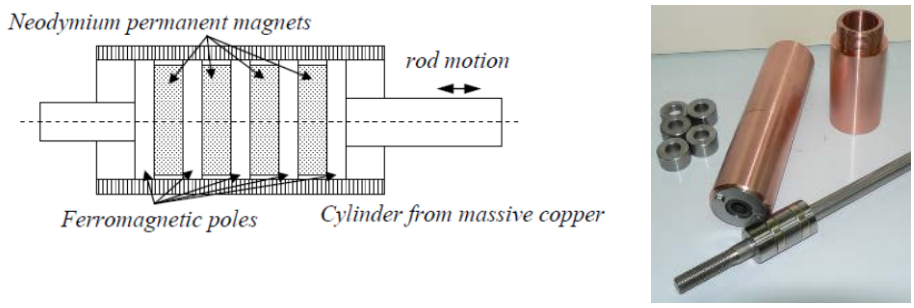

Figure 3. Principle of the EM damper – drawing and testing prototype photography

One of the principles discussed is a passive electromagnetic damper based on eddy currents (see Figure 3). A rod (mover) equipped with a set of neodymium permanent magnet and ferromagnetic poles are moving through a tube made out of a massive copper. The movement of the rod generates eddy currents in the copper tube and force acting

against the motion, which causes required power dissipation. The force can be calculated either analytically or numerically. The principle of such a damper is shown on the Figure3.

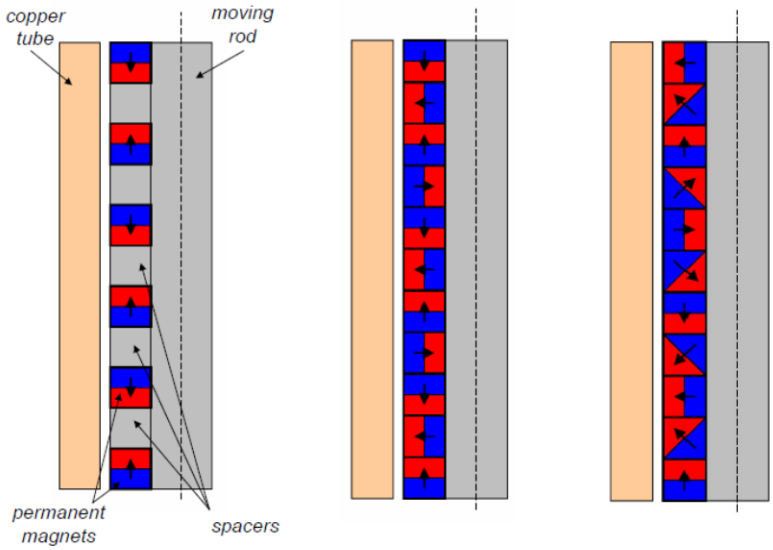

Figure 4. Arrangements of the permanent magnets – from left case 1, 2 and 3

As mentioned above the damping effect is generated by eddy currents arising in the copper stator due to movement of the rod with permanent magnets. Design parameters of such a damper are material and geometrical properties of all components – copper tube, permanent magnets, and pole arrangement (orientation of magnetic field of a single magnet, size of spacers, size of the air gap etc.).

A prototype of such a damper was designed (based on [7]) and manufactured at the author's workplace. Calculations of the magnetic field were done in Comsol Multiphysics and in FEMM software. The focus was given to evaluation of several magnet configurations – see Figure 4.

It was proved, that the magnet arrangement has significant influence to the resulting magnetic field in the air gap, and to the whole system performance.

Three main configurations were studied.

Case 1 consists of axially magnetized neodymium (NdFeB) permanent magnets, ferromagnetic spacers, and non-magnetic rod – see Figure 4a. Case 2 consists of combination of axially and radially magnetized permanent magnets – see Figure 4b. Case 3 is inspired of idea of so called Hallbach's field mentioned in many literature sources. In contains only permanent magnets with axial, radial and axial-radial magnetic field orientation. The magnetic field orientation changes along the rod – see Figure 4c. The main reason for such an arrangement was significant amplification of magnetic field in particular directions, described for Hallbach's field in the literature.

Evaluation of the magnetic field in the air gap was done in SW Comsol Multiphysics and FEMM – see the visualisation example on Figure 5.

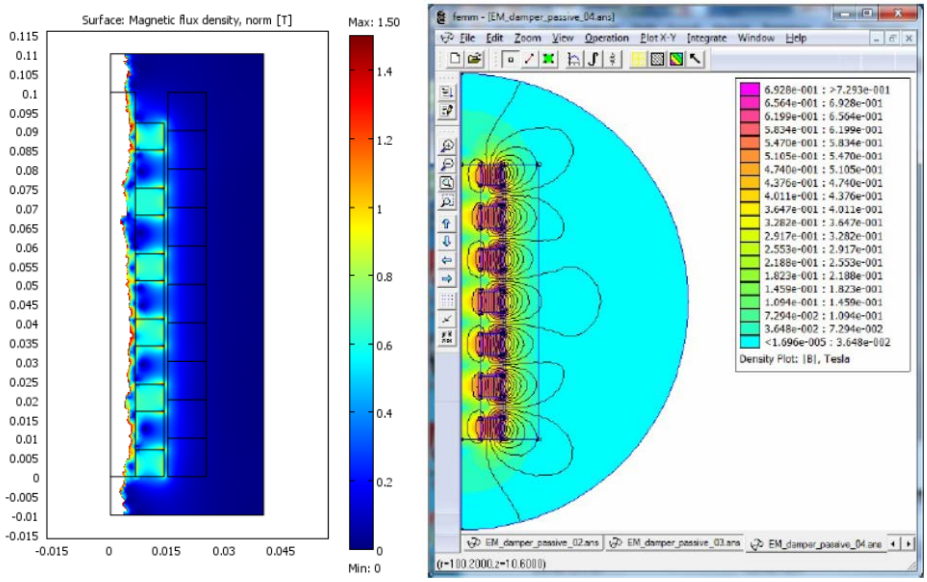

Figure 5. Visualisation of magnetic field for the design case 1 in Comsol Multiphysics and FEMM

For building of the model several unified parameters were used for all the design cases to allow simplicity of evaluation and comparison – see below. Performing of the analysis for the whole range of available parameters would probably give more detailed results, but it was not the goal in this case.

Table 1

Unified model parameters

	Case 1	**Case 2**	**Case 3**
Copper tube outer/inner diameter [mm]	60/30	60/30	60/30
Copper tube length [mm] / modelled length [mm]	300	300	300
Permanent magnet inner/outer diameter [mm]	13/28	13/28	13/28
Permanent magnet length [mm]	7	7	7
Number of permanent magnets	6	13	13
Rod diameter/length [mm]	13/450	13/450	13/450
Spacers outer/inner diameter [mm]	13/28	N/A	N/A
Spacers length [mm]	15	N/A	N/A
Number of spacers	5	N/A	N/A
Air gap between PM and copper tube [mm]	1	1	1
Air gap between spacers and copper tube [mm]	1	N/A	N/A
Permanent magnet material – NiFeB	N40	N40	N40
Rod - non-magnetic steel – relative permeability	1	1	1
Spacers material – soft steel – relative permeability	3000	N/A	N/A

It was assumed, that the damper has the same outer dimensions (copper tube outer diameter and length), i.e. we are comparing dissipation of energy related to the same volume of the damping device. The overall size of the damper is approximately in the same range as common damper size in nowadays personal vehicles.

It was assumed, that the size of PM is the same for all cases. The size (outer and inner diameter and length) was selected from a shopping list of a distributor of permanent

magnets. The reason was to fit the analysis to the particular design configuration, which could be later manufactured.

Model parameters are given in the Table 1.

Table 2

Comparison of design cases

	Case 1	**Case 2**	**Case 3**
Magnetic field in the middle of the air gap avg |B| [T]	0.38	0.56	0.28

The evaluation is given in the Table 2 – showing comparison of magnetic field in the air gap for the studied cases (measured in the middle points of the air gap).

Figure 6 shows an example of calculated magnetic field along the inner surface of copper tube for the Case 1.

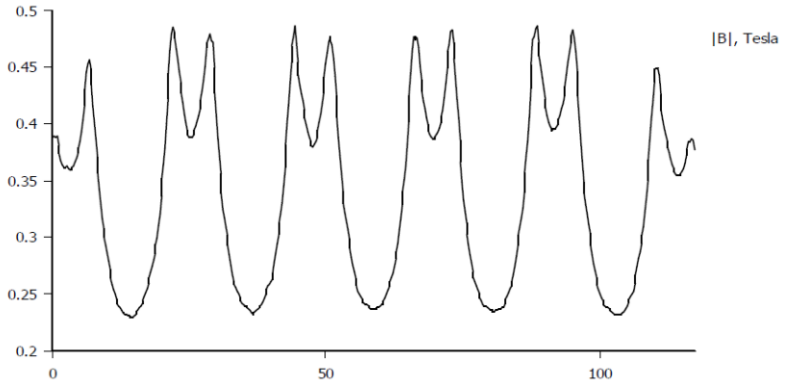

Figure 6. Magnetic field along the inner surface of cooper tube for the Case 1 (x-axis length of tube)

It shows that Case 2 is the best arrangement from the magnetic field intensity point of view. The most complicated and economically less suitable case (Case 3) generates quite low magnetic field in the air gap. Manufacturing of the magnets with given magnetic field orientation would be much expensive than other variants.

Case 1 is the simplest one from the design point of view. Permanent magnets with required magnetic field orientation can be easily purchased on market. Number of permanent magnets is lower than in other cases. Magnetic properties of the Case 1 are lower than in the Case 2, but still acceptable.

When taking into account both functional and economical point of view the Case 1 was selected for development of the first prototype.

2.4. Coiled design, energy recovery

Another principle of the electromagnetic damper is an arrangement similar to linear drive, so called tubular drive (see Figure 7, compare with Figure 3) – passive copper can be replaced by a stator winding or some mechanism can be used to convert linear to rotary motion. There are several principles mentioned in the literature using rotary actuators and planetary gear or various techniques to change linear motion of the rod to the rotary motion

of the actuator. The actuator (either rotary or linear) is in principle an electric drive, either rotary or linear) containing a coil or several coils, which can be fed by constant or variable electric currents. Such an actuator can act as an active or semi-active damper and it also offers ability of energy recuperation. Energy recuperation option can be extremely interesting topic in nowadays electrical vehicles, because of large amount of energy dissipated in the damper during normal operation.

Combination of both principles mentioned above leads to a hybrid damper (see also [7]). Inspired but the text [7] similar damper was designed at author's workplace, and will be manufactured and tested in the nearest future.

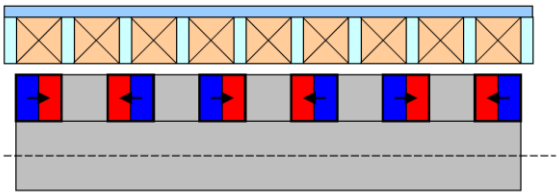

Figure 7. Active and adaptive EM damper with energy recovery option

3. Testing facility for shock absorbers

Mathematical models of the suspension require detail information about the shocks and their behaviour. Understanding of the shock absorber behaviour requires not only virtual testing (modelling and simulation), but also performing several physical tests.

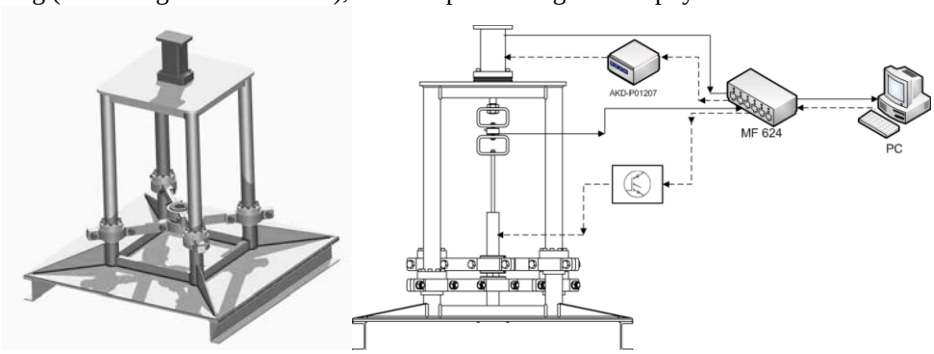

Figure 8. Test rig for automotive shocks design and manufactured at the UWB

Therefore we have built a test device able to measure basic characteristics of the shock absorbers, change properties of the semi-active shocks, understand the behaviour of the dampers and identify parameters further used for simulation models (either simple quarter car model or the full vehicle model). A simple structure (see Figure 8) with four columns for fixing the damper was designed. The rod is driven by linear electric motor. Force sensor is located at the end of the rod. Displacement sensor is included in the drive. Simple amplifier with IGBT transistor driven by analogous voltage from 0 to 10V is used to change the damping characteristics. The whole test rig is controlled from MATLAB via card MF624 and Real Time Target.

The device for testing allows us not only to acquire desired damper characteristic (force-velocity curves) required for modelling and simulation, but also to perform out-of-

the-vehicle tests of shocks with simulated environment and hardware-in-the-loop. The whole system includes the simulation environment mentioned in the paragraph 2, based on SW MATLAB and ADAMS/Car, and the model described in the same chapter.

4. Summary

The paper gives an overview of a design process for a damper for an automotive application, demonstrated on a passive electromagnetic damper. Based on the magnetic field calculations the damper was designed and manufactured. It will be physically tested to evaluate fundamental characteristics of the system and use them in the calculations of mechanical behaviour of the entire system.

5. Acknowledgement

This research was supported by the internal research project SGS-2013-050 at the University of West Bohemia.

6. References

[1] GUGLIELMINO, E.–SIRETEANU, T.–STAMMERS, C. W.–GHITA G.–GIUCLEA, M.: *Semi-active Suspension Control.* Springer, London, 2008.
[2] SAVARESI, S. M.–POUSSOT-VASSAL, C.–SPELTA, C.–SENAME, O.–DUGARD, L.: *Semi-active Suspension Control Design for Vehicles.* Elsevier Ltd., 2010.
[3] RAJAMANI, R.: *Vehicle Dynamics and Control.* Springer, New York, 2006.
[4] FIJALKOWSKI, B. T.: *Automotive Mechatronics: Operational and Practical Issues, Vol. II.* Springer, New York, 2011.
[5] DIXON, J. C.: *The Shock Absorber Handbook.* Second Edition. John Wiley & Sons, Chichester, England, 2007.
[6] SLÍPKA, F.: *Active Systems in Vehicle Chassis.* Diploma thesis. UWB Pilsen, Czech Republic (in Czech), 2012.
[7] BABAK, E.: *Development of Hybrid Electromagnetic Dampers for Vehicle Suspension Systems.* Doctoral dissertation. University of Waterloo, Ontario, Canada, 2009.
[8] ZHANG, P. S.: *Design of Electromagnetic Shock Absorbers for Energy Harvesting from Vehicle Suspensions.* Master Thesis, Stony Brook University, NY, US, 2010.
[9] ZHU, S.–SHEN, W. A.–XU, Y. L.: Linear Electromagnetic Devices for Vibration Damping and Energy Harvesting: Modelling and Testing. *Engineering Structures*, 34, 2012, 198–212.
[10] ZAOUIA, M. at al.: 2D-FEM Modelling of an Electromagnetic Energy Recovery Damper for Vehicle Applications. *International Journal on Electrical Engineering and Informatics*, 6, (1), 2014, 93–106.

Design of Machines and Structures, Vol. 5, No. 1 (2015) pp. 33–38.

MANUFACTURING PARAMETERS DETERMINATION ON BALL NUT GRINDING

GYÖRGY HEGEDŰS

University of Miskolc, Institutional Department of Machine Tools
3515, Miskolc-Egyetemváros
hegedus.gyorgy@uni-miskolc.hu

Abstract: This paper presents a method on the determination of tool profile for internal grinding of ball-nut. The solution is based on the so-called derivation theory, where the parameters of the tool (tilt angle, profile points, approximated profile curve) are determined by numerical methods. The final approximating tool profile is an ellipse-arc where the data points for the approximation are the intersection points of the surface intersection curves. Points of tool profile curves are determined by an initial value problem of ordinary differential equation system (ODE-IVP). The fitting method of approximating ellipses uses a numerically stable noniterative algorithm.

Keywords: *ball-nut, tool profile, approximation, grinding*

1. Introduction

Ballscrew mechanisms are widely used in machine tools and the demand for high-lead ballscrews is increasing due to the high-speed manufacturing. The shape of the ball-nut profile is a gothic arc, which is a symmetrical combined curve of two arcs with equal radius and distance between their centres. These types of balls-nuts are generally manufactured by form grinding (Figure 1), where the grinding tool has corresponding profile [5], for high precision ballscrews lapping techniques are used as well [4]. In case of long and high lead threaded ball-nut the grinding wheel is not tilted at the lead angle of the thread to avoid the collision between the quill and workpiece.

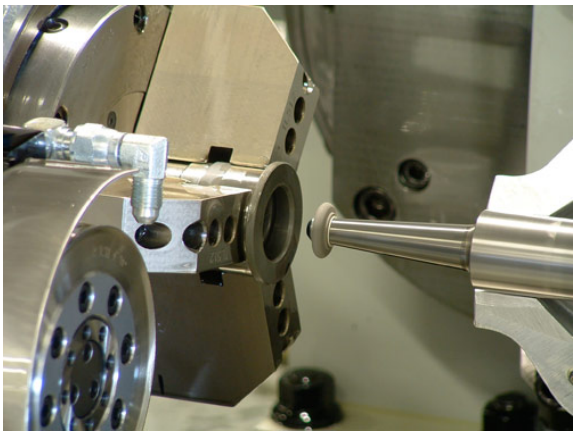

Figure 1. Internal ball-nut grinding with conical tool holder

Due to these conditions the profile obtained is not gothic-arc, because the grinding wheel tends to overcut the thread surface, this problem is well defined i.e. worm and gear

drives [1–3]. There are known methods to obtain the tool surface geometry. Analytical solutions for profiling tools generated by surface enveloping are common and have been used for decades. These solutions are based on the fundamental theorems of the surfaces enveloping such as Olivier's second theorem and Gohman's fundamental theorem [3], [10]. Also, frequently used is Nicolaev's theorem [7], based on the helical movement decomposition. The minimum distance method [9] and the in-plane generating trajectories method [13] are also known profiling methods of this type of tools.

In case of long threaded ball-nut the setting of optimum tilt angle is not possible due to the collision of quill and workpiece (Figure 2). This limits the length of ball-nut which is manufactured. Generally, the length of a ball-nut is specified in advance. In the presented method the quill-inclination is reduced not to meet the internal surface of the workpiece within the specified ball-nut length. For this purpose, the grinding wheel has to be modified with a proper profile, which generates the gothic-arc thread to be obtained [5].

2. Tool tilt angle determination

The tool tilt angle determination is based on a collision detection, or minimum distance computation between the solid bodies of quill and workpiece. Collision detection between cylindrical bodies is widely used in three dimensional mechanical systems, for example machine tools, robots, different mechanisms. Detecting of collision between cylindrical rigid bodies were developed using line geometry by Ketchel and Larochelle [6]. Distance computation between cylinders has four different types according to their three dimensional positions in space (line-line, line-circle, circle-disk and circle-circle distance). Fast and accurate computation method was developed by Vranek [14]. To determine the maximum tilt angle for the grinding the minimum distance determination is required between the tilted quill axis and the edge of the ball-nut represented as a circle (Figure 2).

Determination of minimum distance between the quill and the ball-nut is equivalent with the computation of the distance between the quill axis and the circular edge of the ball-nut.

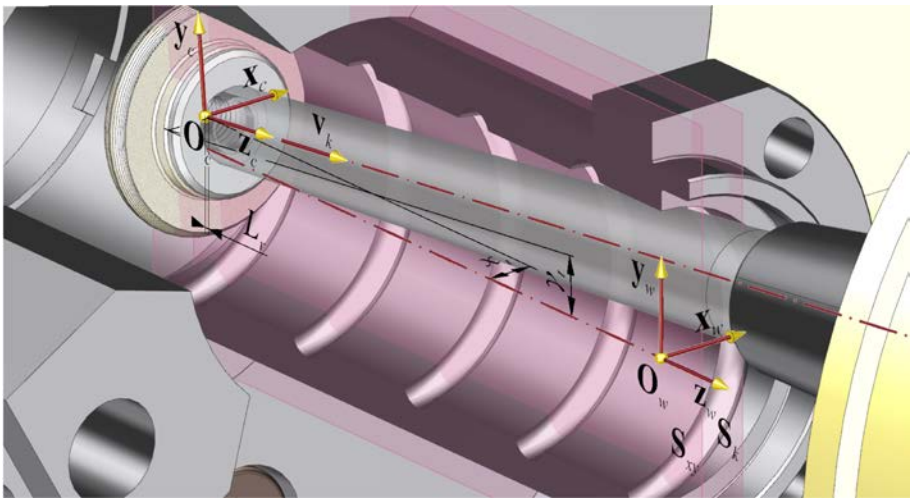

Figure 2. Spatial position of tool-workpiece

The equation of the workpiece circular edge can be written as

$$\mathbf{P}_A = \mathbf{C} + \frac{D_{szt}}{2}\left(\cos(\phi)\mathbf{u} + \sin(\phi)\mathbf{v}\right) \tag{1}$$

where $\phi \in [0, 2\pi]$, $\mathbf{P}_A$ is point of the circle, $\mathbf{C}$ is centre of the circle, D_{szt} is diameter of the quill and $\mathbf{u}$ and $\mathbf{v}$ are unit vectors in the plane containing the circle. The distance between the quill axis and the circular edge is

$$d_{\min}(\gamma_t, t) = b_h - \left(\frac{D_{szt}}{2}\right)^2 + \left|\mathbf{C} - \mathbf{P}_M\right|^2 - D_{szt}\frac{\mathbf{Q} - \mathbf{C}}{\left|\mathbf{Q} - \mathbf{C}\right|} \cdot \left(\mathbf{C} - \mathbf{P}_M\right) \tag{2}$$

where $\mathbf{P}_M$ is a point on the quill axis and $\mathbf{Q}$ is the projection of $\mathbf{P}_M$ on the circle plane and b_h is a safety gap between the quill and the ball-nut. Applying the expressions from [12] a nonlinear equation system can be formulated for the unknown parameters. Differentiate equation (2) with respect the quill axis parameter

$$\frac{\partial d_{\min}(\gamma_t, t)}{\partial t} = 0 \tag{3}$$

the minimum distance between the quill and workpiece can be obtained. Equation (2) and (3) form a quartic nonlinear equation system. Its solutions can be found by root finder algorithms (generally *Newton–Raphson* method is used). In case of conical quill the distance equation is reformulated to

$$d(\gamma_t, \phi) = \left|\mathbf{P}_A - \mathbf{v}_a\right| \sin\left(\cos^{-1}\left(\frac{\left(\mathbf{P}_A - \mathbf{v}_a\right)\mathbf{v}_k}{\left|\mathbf{P}_A - \mathbf{v}_a\right|\left|\mathbf{v}_k\right|}\right) - \beta\right), \tag{4}$$

where $\mathbf{v}_a$ the direction vector of the conical surface generatrix, β half opening angle of the cone. The minimum distance between the conical surface and the workpiece edge is

$$\frac{\partial d_{\min}(\gamma_t, \phi)}{\partial \phi} = 0. \tag{5}$$

Due to the reduced quill-inclination the grinding wheel has to be modified with the proper profile depends on the workpiece parameters. In the next section the method of tool profile generation is described.

3. Tool profile generation

In this section a numerical method for the determination of tool profile of grinding tool is described. The surface intersection method is based on the solution of system of ODEs. The parametric equation of the internal gothic arc ball-nut surface is

$$\mathbf{S}_b(u, v) = \mathbf{h}(u) + R_{pr}\left[\mathbf{b} \cdot \sin(v) - \mathbf{n} \cdot \cos(v)\right], \tag{6}$$

where $\mathbf{h}(u)$ is the parametric equation of helical curve of swept surface, $\mathbf{b}$ is the binormal, $\mathbf{n}$ is the normal vector of helical curve and R_{pr} is the radius of gothic arc. The parametric equation of the tool plane is given by

$$\mathbf{S}_k(q, t) = \mathbf{O}_c + q \cdot \mathbf{z}_c + t \cdot \mathbf{x}_c. \tag{7}$$

The intersection curve of two surfaces is determined by

$$\mathbf{C}(u, v, q, t) = \mathbf{S}_b(u, v) - \mathbf{S}_k(q, t) = \mathbf{0}. \tag{8}$$

If a direction vector can be found such that is orthogonal to all gradients, than the intersection curve can be traced by following this direction. This orthogonal vector is determined by a modified *Jacobian* determinant

$$\mathbf{P}(u,v,q,t) = \det\begin{bmatrix} \mathbf{e}_u & \mathbf{e}_v & \mathbf{e}_q & \mathbf{e}_t \\ & J_C(u,v,q,t) & & \end{bmatrix}, \tag{9}$$

where $J_C(u,v,q,t)$ is the *Jacobian* of the intersection curve formed by equation (8). The above formula determines an *ODE-IVP* system. The initial value vector is determined by fixing one of the parameters and solving for the rest by *Newton–Raphson* method. After the appropriate starting point found the *ODE* system is solved numerically by 4–5 order *Runge–Kutta* algorithm [8].

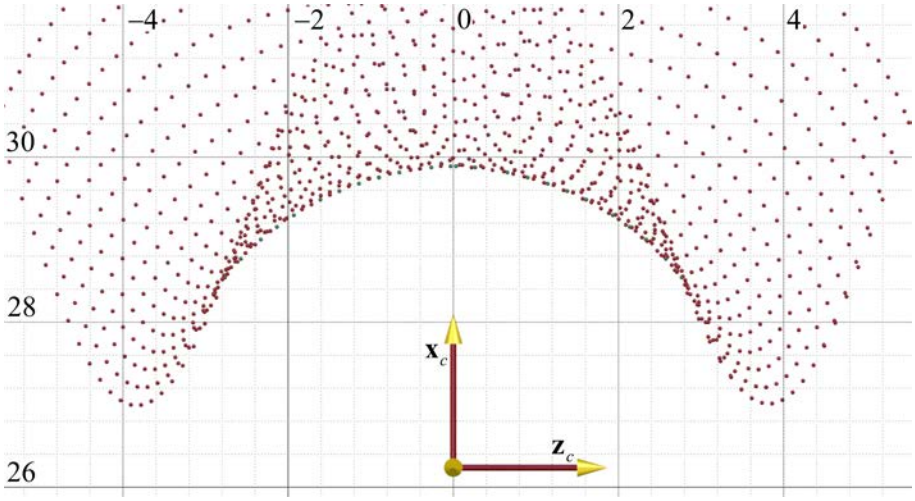

Figure 3. Surface intersection points of Runge–Kutta algorithm

The number of surface intersections determines the number of ODEs to solve (Figure 3). Obtaining the points of intersection curve an approximated ellipse-arc is determined by a numerically stable non-iterative algorithm, described in the next section.

Starting and ending points and the intersection points of the ellipse-arcs are requested to generate tool profile. Figure 3 shows the intersection points, the profile and noise points transformed into *xz plane* of the tool. Ellipses are special cases of general conics which can be described by an implicit second order polynomial

$$F(x,z) = ax^2 + bxz + cy^2 + dx + ez + f = 0, \tag{10}$$

where *a, b, c, d ,e ,f*are coefficients of the conic and $b^2-4ac < 0$ is a further constraint for ellipse. The *algebraic distance* $F(x,z)$ rewritten in vector form

$$F(\mathbf{x}) = \mathbf{x}\cdot\mathbf{a} = 0. \tag{11}$$

The fitting of a general conic to a set of points $(x_i; z_i)$; $i = 1\ldots n$ may be approached by minimizing the sum of squared algebraic distances of the points to the conic which is represented by coefficients **a**:

$$\min\sum_{i=1}^{n} F(x_i,z_i)^2 = \min\sum_{i=1}^{n}\left(F(\mathbf{x_i})\right)^2 = \min\sum_{i=1}^{n}\left(F(\mathbf{x_i}\cdot\mathbf{a})\right)^2 \tag{12}$$

Equation (12) can be solved directly by the standard least squares algorithm, but the result is a general conic. In specific ellipse case further constraint required to fit an ellipse to the

filtered profile points [15]. An improved fitting algorithm is proposed and implemented in the appropriate MATLAB code [11].

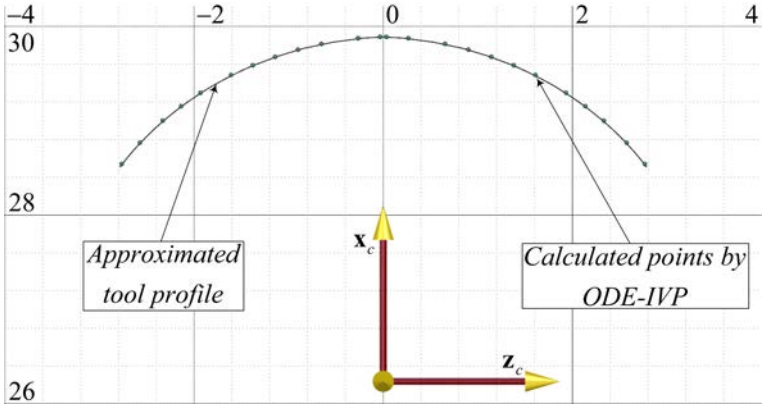

Figure 4. Points for profile approximation, d = 50mm, p = 30mm

There are two noise sections among these collected points which have to be filtered out. The limiting point of undercutting is calculated by

$$\left|\mathbf{B}(t)_{i-1,i} - \mathbf{F}_1\right| + \left|\mathbf{B}(t)_{i-1,i} - \mathbf{F}_2\right| - 2a = 0 \tag{13}$$

where $\mathbf{B}(t)_{i-1,i}$ is the *i*-th cubic *Bezier* curve ($t = 0…1$, $i = 1…n$, n the number of intersection curves), $\mathbf{F}_1$ and $\mathbf{F}_2$ focus points of fitted ellipse on the intersection points of ellipse-arcs between the minimum point of intersection points and ending point of tool profile (this point calculated from ball-nut parameters), a semi-major axis of the fitted ellipse-arc. The solution of nonlinear equation (13) is determined by *Newton–Raphson* method. The final approximated tool profile is generated by mirroring of the two approximating cubic *Bezier* curve and ellipse-arc (Figure 4).

4. Summary

This paper presents numerical applications for the profiling of grinding tools for the generation of gothic-arc helical surfaces with constant pitch, based on derivation theory and surface-surface intersection. The proposed methods used the capabilities of the MATLAB mathematical computing environment. The results was obtained in numerical form and confirmed by graphically. The final approximating tool profile is an ellipse-arc where the data points for the approximation was the intersection points of the surface intersection curves determined by an initial value problem of ordinary differential equation system (ODE-IVP).

The accuracy of the results depends on the Runge–Kutta step size used for to solve the ODE-IVP. The method is generic that it can be used for different geometrical shapes and different tool profile.

5. Acknowledgement

This research was supported by the European Union and the State of Hungary, co-financed by the European Social Fund in the framework of TÁMOP 4.2.4. A/2-11-1-2012-0001 ‘National Excellence Program’.

6. References

[1] DUDÁS, I.: *The Theory and Practice of Worm Gear Drives.* Butterworth–Heinemann, 2004, 320.

[2] DUDÁS, L.: New Way for the Innovation of Gear Types. In: *Engineering the Future, Chapt. 6.* Sciyo, Croatia, 2010, 111–140.

[3] LITVIN, F. L.–FUENTES, A.: *Gear Geometry and Applied Theory.* Cambridge University Press, 2004, 801.

[4] GUEVARRA, D. S.–KYUSOJIN, A.–ISOBE, H.–KANEKO, Y.: Development of a New Lapping Method for High Precision Ball Screw (1st report) – Feasibility Study of a Prototyped Lapping Tool for Automatic Lapping Process. *Precision Engineering Journal of the International Societies for Recision Engineering and Nanotechnology,* 25, 2001, 63–69.

[5] HARADA, H.–KAGIWADA, T.: Grinding of High-lead and Gothic-arc Profile Ball-nuts with Free Qill-inclination. *Precision Engineering,* 28, 2004, 143–151.

[6] KETCHEL, J.–LAROCHELLE, P.: Collision Detection of Cylindrical Rigid Bodies Using Line Geometry. In: *Proceedings of the 2005 ASME International Design Engineering Technical Conferences,* ISBN: 0-7918-4744-6, California, September 2005, 3–13.

[7] LUKSHIN, V. S.: *Theory of Screw Surfaces in Cutting Tool Design.* Machinostroyenie, Moscow, 1968.

[8] MATHEWS, J. H.–FINK, K. D.: *Numerical Methods Using MATLAB* (Third Edition). Prentice Hall, 1999, 680.

[9] OANCEA, N.: *Surface Generation Through Winding, Volume 2. Complementary Theorems.* "Dunărea de Jos" University Publishing House, Galați, 2004.

[10] RADZEVICH, S. P.: *Kinematic Geometry of Surface Machining.* CRC, London. 2008.

[11] HAL, R.–FLUSSER, J.: Numerically Stable Direct Least Squares Fitting of Ellipses. In: *The 6th International Conference in Central Europe on Computer Graphics and Visualization,* 21 (5), 1998, 59–108.

[12] SCHNEIDER, P. J.–EBERLY, D. H.: *Geometric Tools for Computer Graphics.* Morgan Kaufmann Publishers, San Fransisco, 2003, 1056.

[13] TEODOR, V.: *Contribution to the Elaboration of a Method for Profiling Tools – Tools which Generate by Enwrapping.* Lambert Academic Publishing, Saarbrücken, Germany. 2011.

[14] VRANEK, D.: Fast and Accurate Circle–circle and Circle–line 3D Distance Computation. *Journal of Graphics Tools Volume,* 7 (1), 2002, 23–32.

[15] GANDER, W.–GOLUB, G. H.–STREBEL, R.: Least-squares Fitting of Circles and Ellipses. *BIT Numerical Mathematics,* 34 (4), 1994, 558–578.

Design of Machines and Structures, Vol. 5, No. 1 (2015) pp. 39–46.

FEM MODELLING OF CONTACT INTERACTION BETWEEN WHEEL AND SUPPORTING

VITALIY KURDYUK–NATALYA VOLSKAYA

Moscow State Industrial University
115280, Avtozavodskaya st. 16, Moscow, Russia
v.kurdyuk@gmail.com,

Abstract: Modelling of contact interaction of wheel and the supporting surface is an important problem for the vehicle design. Paper considers the option of modelling the wheel, as well as methods of processing the calculation results of the dynamic contact interaction for the main evaluation parameters. A version of simulation cord and breaker of the shell element is proposed. The adequacy and effectiveness of the proposed method of processing the results of contact interaction of the wheel and the bearing surface are shown.

Keywords: *car, wheel, tire, contact, modelling of contact interaction, CAD, FEM, ANSYS, LS-DYNA*

1. Introduction

As part of his thesis on the topic of choosing the optimal parameters of suspension system, depending on the operating conditions faced with the task of processing the results of modelling of contact interaction of the wheel and the supporting surface. From the perspective of permeability, the most important parameters are the contact interaction are peak pressure at the contact patch, the average pressure at the contact patch, the coefficient of rolling resistance, width and depth track.

The software package ANSYS LS-DYNA was chosen to model the contact interaction between the wheel and the bearing surface because it is one of the most advanced tools for solving problems of this kind, well in the work of the leading manufacturers of wheel tire companies (including Michelin, Goodyear). This program is designed to simulate nonlinear problems involving large deformations.

2. Simulation of finite-element model

The system contains two parts: tire (p. 1, Figure 1) and supporting surface (p. 2, Figure 1). In this case it is not attempt to obtain quantitative results, a qualitative assessment only and analysis of it. That is why the supporting surface is represented by the height of one parallelepiped element and superior in size to the dimensions of the wheels 50%.

As the material of the supporting surface (p. 2, Figure 1) is selected concrete with following characteristics: elasticity modulus $2 \cdot 1010Pa$, Poisson ratio 0.2, density 2500 kg/m³. Modell were performed by volume elements solid164 type.

Wheel modelled from several parts: belt (p. 1, Figure 2), cord (p. 2, Figure 2), rubber part of tyre (p. 3, Figure 2), bead (p. 4, Figure 2), rim (p. 5, Figure 2), disk (p. 6, Figure 2).

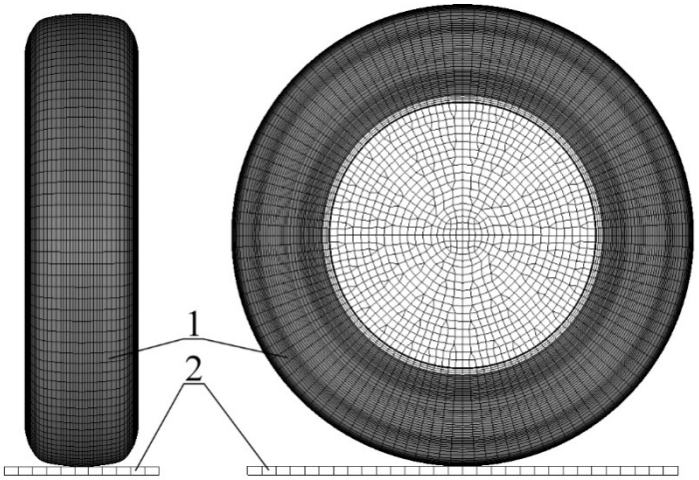

Figure 1. Finite-element model of the system
1 – tyre; 2 –supporting surface

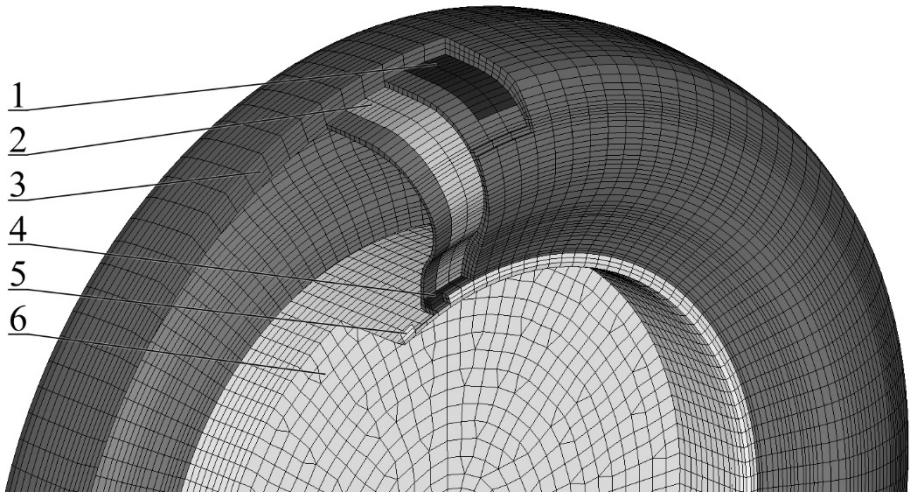

Figure 2. Finite-element model of tyre
1 – belt; 2 – cord; 3 – rubber part of tyre; 4 – bead; 5 –rim; 6 – disk

Belt (p. 1, Figure 2) and cord (p. 2, Figure 2) were performed by shell elements shell163 by orthotropic material (carbon steel) with following characteristics by main direction: elasticity modulus $2.1 \cdot 1011Pa$, Poisson ratio 0.28, density 7800 kg/m³. In two other directions of the modulus of elasticity is $9.3 \cdot 1010Pa$. The thickness of the elements is 0,025 mm.

Thickness and elasticity modulus elements on secondary directions chosen so to ensure the rigidity and weight [1] equivalent to the corresponding parameters of the cord and the belt composed of steel filaments (Figure 3).

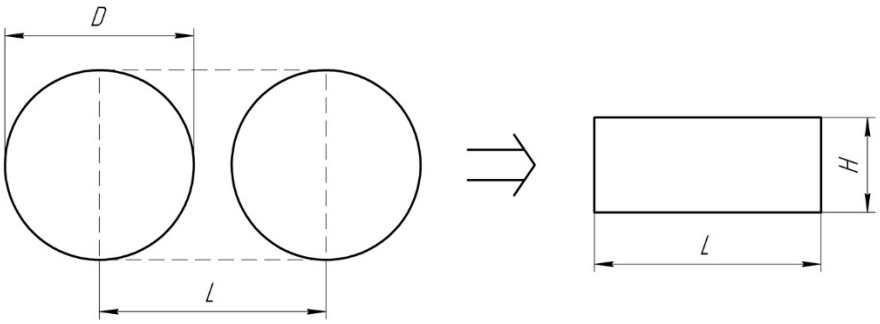

Figure 3. Converting square of cord to equivalent to the area of a rectangle

In the case of small dimensional deformations (within the elastic zone, where in Hooke's law is valid), the stiffness can be defined as the product of modulus of elasticity (in tension, compression and bending) or the shear modulus (shear and torsion) to the relevant geometrical characteristics of the element cross section. In the case of bending it is the axial moment of inertia. Belt and cord works on bending and stretching in this task [0]. The equivalence of the tensile stiffness is provided by the equality of cord steel filaments area and the equivalent rectangle:

$$H = \frac{\pi D^2}{4L} \tag{1}$$

The equivalence of the bending stiffness is determined by the product of the modulus of elasticity to the polar moment of inertia for both sections. This means that:

$$E_{eq} = \frac{12L^2}{\pi^3 d^2} E_{steel} \tag{2}$$

The flexural rigidity of belt and cord in the transverse direction is much less than in a longitudinal because weaving structure where rigid steel filaments in this direction are connected kapron flexible filaments.

Since the thickness of the equivalent cross-section has been determined previously, the equivalent modulus of elasticity in the transverse direction define equal to experimentally obtained.

Rubber part of tire (p. 3, Figure 2) was performed by solid elements solid164 type by Mooney–Rivlin model (used to modelling hyper elastic elastomeric materials such as rubber). Material characteristics: Poisson ratio 0.499, density 1200 kg/m³. Size and load curve of the sample correspond to the experimentally obtained data.

Bead (p. 4, Figure 2) was performed by solid elements solid164 type from carbon steel material. It has the following characteristics: elasticity modulus $2.1 \cdot 1011Pa$, Poisson ratio 0.28, density 7800 kg/m³.

Rim and disk (p. 5 and p. 6, Figure 2) were performed by shell element shell163 from carbon steel material with following characteristics: elasticity modulus $2.1 \cdot 1011Pa$, Poisson ratio 0.28, density 7800 kg/m³. In this task the solution accuracy is not required. Therefore, to simplify model the thickness of the element is set to 5 mm in all sections.

Assumptions: this model is intended for the qualitative assessment of contact interaction of the wheel and the bearing surface, so all the elements that do not affect the stiffness of the tire were modelled with simplifications and their mechanical properties are set to the

reserve. The bead is made of steel and considerably larger than the prototype. It has no effect on the stiffness of the tire because of the distance from the contact patch. But this simplification reduces the complexity of the simulation.

Rim and disk executed by the simplified geometry, so that loads are applied to node in the geometric centre of the wheel assembly. The thickness of the elements was chosen higher than necessary to eliminate the influence of the rigidity of the disk on the interactions of tire and supporting surface. In this model they perform an auxiliary function.

Consolidations and loads: the support surface mounted on axes X, Y and Z in the lower part. Disk nodes have restrictions on lateral movements.

To the inner surface of the rubber part of the tire pressure of 200 kPa is applied. To the central disk node attached downward direction vertical force 1750 N. The same node attached torque 100 Nm in the direction of the wheel rolling. To all nodes of the model applied acceleration of gravity g.

Due to the fact that a model created for the qualitative analysis of the interaction and does not require the precise values he tread pattern is absent.

3. Method of results calculation process

To determine the width and depth of the track is required to obtain data on the movement of the reference points of the surface. It will be enough to get the data from all three points – vertical movement of the node in the centre of track and coordinates of nodes on opposite edges of the gauge (the track width is absolute value of their difference).

To obtain the desired peak value of pressure at the contact patch, the average pressure at the contact patch, the coefficient of rolling resistance is required to convert data received from the pattern of pressure distribution in the contact patch.

This picture is available in ANSYS and LS-DYNA postprocessor: Plot > Results > Contour plot > Element solution > Stress > Y-Component of stress.

For the convenience of processing the results should make the colour scale legend in the form of shades of grey from black (zero pressure) to white (maximum pressure). To do this, create a new scale: PlotCtrls > Style > Colours > Create Colour Map. The preferred will create 16 shades of grey and even pitch in brightness. If possible, one must create 256 levels.

For ease of processing it is recommended to set a scale so that the minimum value is negative, so that:

$$\min = -\frac{\max}{n-1} \tag{3}$$

where max is the maximum value of the study, n is the number of grey levels.

In this case, it turns out that each gradation (except the first one corresponding to zero and negative values) corresponds to the value:

$$p_i = \frac{\max}{n-1}(i+1) \tag{4}$$

where i is number of level.

Then one can bring a picture of the pressure distribution on the screen and save the image: PlotCtrls > Capture Image > File > Save as > select the file name and format bmp (bitmap – no compression). It is recommended to use the maximum resolution of the monitor ANSYS expands the window to full screen and hide all the tool windows.

Next, in a graphics editor (e.g.: GIMP 2.8) one must clear the corresponding section of the wheel is not involved in the contact (make them black tool brush, which corresponds to zero pressure) and save the file in PBM p2 (portable bitmap encoded in ASCII [3]): File > Export > Drawing PGM > Export > Text (ASCII) > Ok.

At this stage it is possible to reduce the size of an image without carrying the information about voltages (black squares), to reduce the size of the matrix and increase the rate of calculating (Part II, Figure 4).

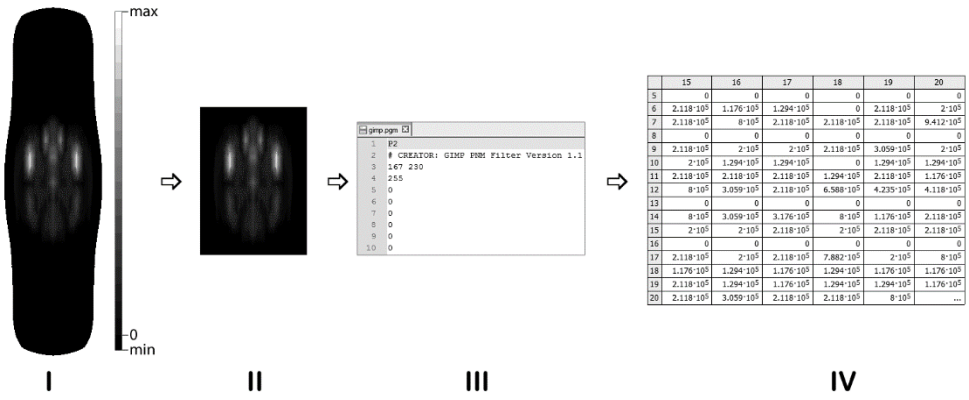

Figure 4.The processing steps of calculation results
1 – original picture of the stress distribution; 2 – treated pattern of stress distribution; 3 – vector format data PGM; 4 – matrix stress distribution

The resulting file should be opened in a text editor (e.g.: Notepad++). Figure 5 shows a sample file PGM. In it, the first line p2 represents the version of the format (in this case, grayscale, recorded in the encoding ASCII), the third row contains information about image size (number of columns {col} and row {row}, respectively), and the fourth – the depth of colour {depth} [0] (255 means that each pixel can have a brightness of 0 to 255). The fifth and next to the end of file – brightness {data}.

gimp.pgm

```
1  P2
2  # CREATOR: GIMP PNM Filter Version 1.1
3  13 5
4  255
5  247
6  240
7  246
```

Figure 5. Listing of the PGM file

The resulting data can be transferred into the program, which make calculation (MathCAD, Excel etc.).

The variable data contains a column of data (Part III, Figure 5), which should be transformed into a matrix of brightness:

$$lightness_{i,j} = \frac{data_{i(row-1)+j}}{depth} \tag{5}$$

where j varies from 1 to row, i varies from 1 to col.

Now lightness is a matrix of relative brightness. Multiplying it by the maximum pressure {max} of the legends of the initial picture of the stress distribution (Part I, Figure 5) we obtain the matrix of the pressure distribution in the contact patch (Part IV, Figure 5).

In the event of a major partitioning into finite elements model the pressures can be calculated manually using the colour picker tool in your photo editor and putting it into line value from the legend of the original image.

Define the contact area:

$$S = \sum_1^n \sum_1^m p_{Heaviside} l^2 \tag{6}$$

where n, m are the number of rows and columns in the matrix of pressure values, $p_{Heaviside}$ is the matrix of pressure values, each element of which is equal to one if the corresponding element of a non-zero pressure (using the Heaviside step function [0]), l is the length corresponding to one pixel of the image pattern pressure distribution in the contact patch.

This length is determined by the ratio of the size of the model in millimetres corresponding to the size of the image in pixels. For this purpose it is convenient to create a finite element model of three-element beam length of 0.1 m (or any other comparable with the characteristic dimensions of the model) in the direction of the principal coordinate and consolidate all of their components from moving. They are conveniently situated away from the main model, so they do not overlay on the deformed model after calculation but were visible. The size of the image in pixels can be defined in a graphics editor.

Defining the total vertical force exerted by the wheels on the supporting surface:

$$F_\Sigma = \sum_1^n \sum_1^m pl^2 \tag{7}$$

where p is the pressure of the matrix (obtained by the mapping results to calculate pressure LS-DYNA). In the stabilized mode, this force must be equal to the sum of the vertical forces acting on the centre of the wheel and the mass of the wheel.

Then the average pressure in the contact patch will be determined by dividing the total force to the area of the contact:

$$p_{avg} = \frac{F_\Sigma}{S} \tag{8}$$

Peak pressure in the contact spots will be determined as a function of the maximum:

$$p_{\max} = \max(p) \tag{9}$$

The coefficient of rolling resistance is determined by the formula:

$$f = \frac{M(r_K - r_{dyn})}{F_\Sigma r_K r_{dyn}} + \frac{a}{r_{dyn}} \tag{10}$$

where M is the torque, r_K is the free wheel radius (defined geometry), r_{dyn} is the dynamic wheel radius (calculated as the difference between the vertical coordinates of the central disk node (O) and a node located in the contact), a is the longitudinal displacement of the centre of pressure relative to the projection in the centre of the wheel contact patch.

Calculate longitudinal displacement of the centre of pressure as the difference of the distance between the longitudinal coordinates of the centre of the wheel (O) and the farthest node of the contact (L_1) and the distance from the node to the centre of pressure (O_p) of the contact (L_2). L_1 value is determined in ANSYS: TimeHistPostpo >AddData > Nodal

Solution > DOF Solution > X-Component of displacement > one need to choose the node > List Data > after this, select the value corresponding to the time when the oscillations died down and the wheel moves in steady mode. L_2 value is determined from the pressure distribution matrix according to:

$$L_2 = \frac{M_p}{F_\Sigma} \tag{11}$$

where M_p is the moment created by the pressure relative to the farthest node of the contact:

$$M_p = l^2 \sum_1^n \sum_1^m \left[p_{i,j} \left(il + \frac{l}{2} \right) \right] \tag{12}$$

4. Results

Processing of the results gave the following values (Figure 6): col = 167 is the number of columns in the contact patch pattern; row = 230 is the number of rows in the contact patch pattern; depth = 255 is the brightness depth; max = $3 \cdot 10^6$ Pa is the maximum pressure in the contact patch (in legend); l = 0.59 mm is the length corresponding to one pixel; S = 66.9 cm^2 is the contact patch area [62]; F_Σ = 2580 N is the integrated force in contact patch [2450]; p_{avg} = 386 kPa is the average pressure at the contact patch [395]; p_{max} = 2860 kPa is the peak pressure in contact patch; f = 0.016 is the coefficient of rolling resistance [0.015–0.018].

The numbers in square brackets are the theoretical values. As you can see, all the values are relatively minor error theoretical except peak pressure. Lots of peak pressures under the edge of the belt, at the transition to the sidewall of the tire tread. This corresponds to the observed picture of the stress distribution in the contact patch.

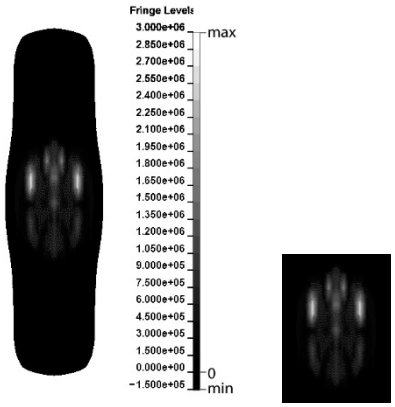

Figure 6.The results of the calculation.contact pressure

5. Conclusion

The calculation results show that the proposed finite-element model of the wheel and the method of processing the results of the calculation are adequate and can be applied in the

future. The error in the estimated parameters of the contact interaction of the wheel and the bearing surface does not exceed 10%.

The calculation showed that the main novelty of the model (modelling cord and breaker of the shell element) is admissible and can reduce the dimensionality of the model, thereby increasing the speed of calculation, by reducing the number of beam elements.

Evaluation of contact interaction parameters were calculated by hand and by the proposed method. The parameters obtained by the proposed method have a smaller error relative to the experimental data.

6. References

[1] *Stiffness,* http://en.wikipedia.org/wiki/Stiffness.
[2] *Heaviside step function*, http://en.wikipedia.org/wiki/Heaviside_step_function.
[3] *Portable anymap,* http://en.wikipedia.org/wiki/Portable_anymap.

Design of Machines and Structures, Vol. 5, No. 1 (2015) pp. 47–52.

DESIGNERS AND SUSTAINABILITY

IVANA MAZÍNOVÁ

University of West Bohemia, Department of Machine Design
Czech Republic, Plzeň (Pilsen)
mazini@kks.zcu.cz

Abstract: The article deals with Sustainable Development from the point of view of the designer who selects materials for a given product. Is it possible to objectively assess the impact of our actions on the environment 100 years from now? One of possible methods for assessing the impact of the selection of materials on the environment is given in the case study.

Keywords: *Sustainability; Triple Bottom Line accounting; analysing sustainable developments; Corporate Social Responsibility*

1. Introduction

The concept of sustainable development is understood in different ways by different people, often depending on their needs for pursuing their own interests. Some politicians abuse the term for political purposes, and some large corporations use the term ‘sustainability’ only for purposes of growing their business. On the other hand oil companies understand the term sustainable development in relation to their future as a ‘time after oil’. Generally it can be said that the majority of people think of sustainability as the unlimited use of all available technologies for the growth of gross domestic product whilst reducing the undesirable effects on the environment (for example, reduction of carbon emissions). And then there are those who do not trust this approach, who see the free market as the cause of environmental problems, which is the continuous driving force behind the growing threat to an unsustainable future. Sustainable development is seen as equilibrium, not growth. Between these two points of view there are many other opinions. We are living at a time when neither conclusive proof – nor one side of the argument, can be obtained – only time will tell.

2. Sustainability

So what then is sustainability? It depends on your point of view – the scale, whether it is local or global, and the time frame – whether it is weeks, years, or centuries.

Sustainable development is a means of developing human society which is carried out in agreement with economic and social progress whilst fully preserving the environment. The main objective of sustainable development includes the preservation of the environment for future generations with as little change as possible. The principles of sustainability are set out in standard CSN 01 0391, which was released in October 2013, entitled ‘Corporate social responsibility management system – Requirements’ [4]. The introduction of this standard states:

‘Specifically, the integration of social responsibility manifests itself by integration of positive attitudes, practices and programmes into an organization’s strategy at the level of top management. It requires a shift in the view of their social role from the level of “profit

only" to a broader perspective in the context of the often-mentioned three pillars "P" – People – Planet – Profit'.

Unfortunately many firms see social responsibility as a fashionable trend a means for self-promotion.

The Figure 1 shows sustainability represented as the 'Triple Bottom Line'.

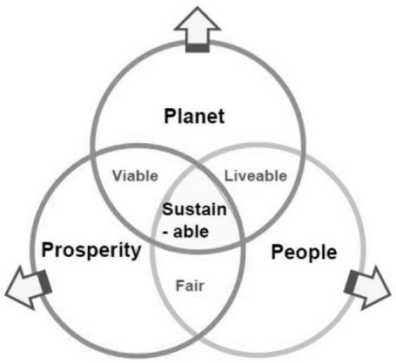

Figure 1. Triple Bottom Line [5]

This apparently simple diagram is very hard to implement in practice. It demands a detailed analysis of single actions ('articulations') in a system and a subsequent synthesis of the facts and, most significantly, a large dose of common sense.

How should engineers approach the issue of sustainability? What and how should we teach students? Thanks to a certain Czech president (and not only him), the overwhelming opinion in the Czech Republic is that there is no threat. Technical specialists tend to see this issue as something for philosophers. Questions such as the following are regarded by technical specialists as, at the very least, strange:

How long can economic growth, which is always exponential, be sustainable?

Is strong economic growth compatible with the needs of today's and future population?

Is sustainable development (in the context of the continuously widening gap between rich and poor countries) actually achievable?

And is it really in our interests to worry about what comes after us?

3. Sustainability from the viewpoint of engineers

I would like to share with you a rational analysis of sustainability issues, conducted by Professor Ashby et al. from the perspective of material selection [5]. How is it done? By separating the rings and developing their meaning (Figure 2).

There are many different proposals ("articulations") that are used to promote a "Sustainable Development". Proposals are submitted from various stakeholders. Among the stakeholders include governments, the public, local communities, owners, manufacturers, suppliers, trade unions, customers, lobbyists, investors, national press, managers. They have their interests and their power of influence. Thereby get their proposals logically into conflict. Due to the length of the contribution skip lists the main proposals of individual stakeholders. Their interests can be derived following main categories (meaning still in terms of material selection):

- Materials(manufacture supply chain, life cycle)
- Environment(carbon release, air, water, land)
- Design-energy (energy efficiency, function, performance, safety)
- Legislation(awareness, compliance, reporting)
- Society(social equity, education, health)
- Economics (cost, benefit).

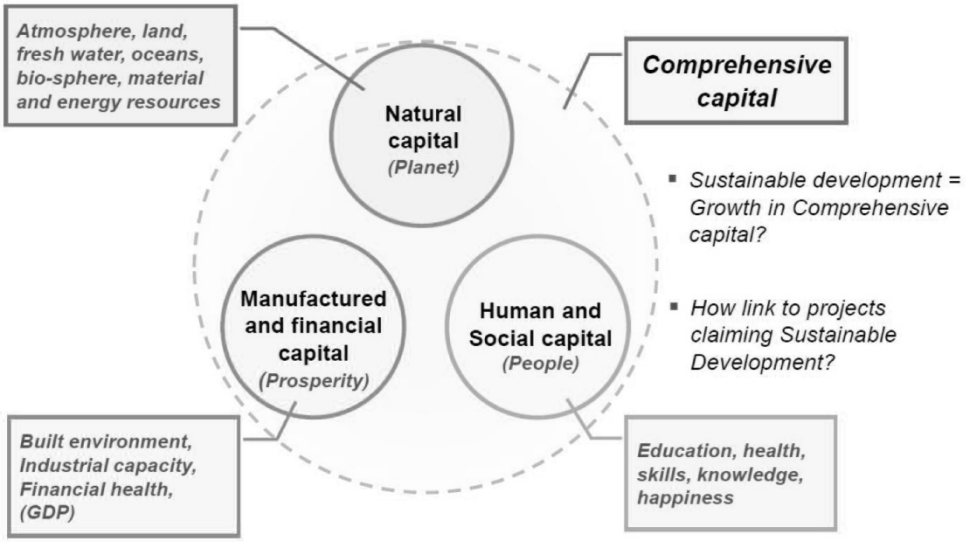

Figure 2. Macro-economic view: the Three Capitals [5]

Individual proposals ("articulations") of stakeholders must be systematically explored. Generally, you can define a method to assess the sustainability of these five steps:

Step 1: Clarify objective
Step 2: Stakeholders analysis
Step 3: Fact finding (objective)
Step 4: Debate impact (subjective)
Step 5: Reflection

4. Case study: the electric car

Practical application of the method is demonstrated on the electric car. Is the electric car sustainable?

Step 1: Clarify objective

Based on these facts (background): Global car production is 60 million units per year; 15% of CO_2 release comes from car; Governments targets are 10% electric by 2020. Prime objective is decarbonize road transport. Scale is 8 million cars/year by 2020.

Step 2: Stakeholders and concerns

- National and local government – carbon targets
- Car makers and distributors – sales
- Battery makers – supply chain, recycling
- Labour Unions – employment, rights
- Drivers, Automobile Association – range anxiety, cost
- Environmental campaigners – carbon footprint

Battery makers have strongest influence and greatest interest.

Step 3: Fact finding

The strongest stakeholder interests split into major categories stakeholder interests, which have been described above:

- Material supply chain – Lithium
- Energy – batteries
- Legislation – battery directive
- Environment – CO_2 footprint
- Society – range anxiety
- Economics – acceptance of cost

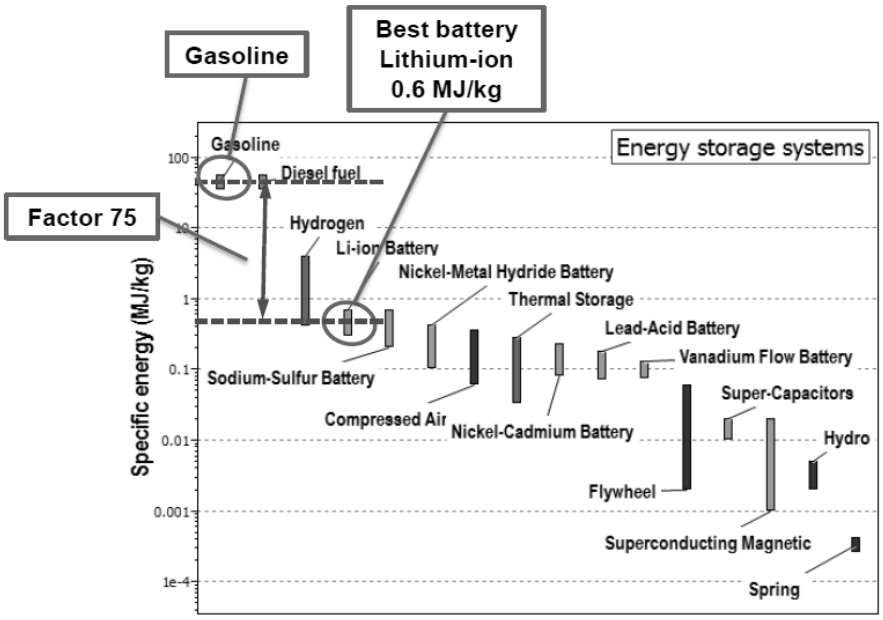

Figure 3. Bar chart – Energy storage systems [2]

Material – Consumption per car is 7.3 kg Lithium, if the goal of 8 million cars per year, consumption is 58,400 tons per year Lithium. Annual world production of Lithium in 2011 was 34,000 tons. From these facts it follows that the requirement for 2020 would be 160% of current world production.

Energy – What are alternative batteries? Bar chart in Figure 2 created using the CES software (link) shows the energy density of materials. The graph shows that the Lithium-ion battery has the highest energy capacity. Energy density of batteries is much smaller than gasoline.

Regulation – EU battery directive is no batteries to landfill.
Society and stakeholders concerns – The travelling distance is limited by the battery weight and cost. 500 km range requires more than half tonne Li-on battery. It follows that battery weight is proximately 1 kg/km. Cost at todays prices $42,000 (http://evobsession.com/electric-cars-2014-list/)

Environment – Can prime objective be met? Will be decarbonizes road transport?
The battery must be recharged from the National Grid (gas/coal fired) – the carbon footprint resulting in the production of electricity from gas is 140 g/MJ.
Delivered energy to propel small car is 0.6 MJ/km.
Efficiency of battery – electric motor set is 85%.
It follows that carbon footprint of electric car is 140 x 0.6 / 0.85 ≈ 100 g/km.

Step 4: Impact on the three capitals

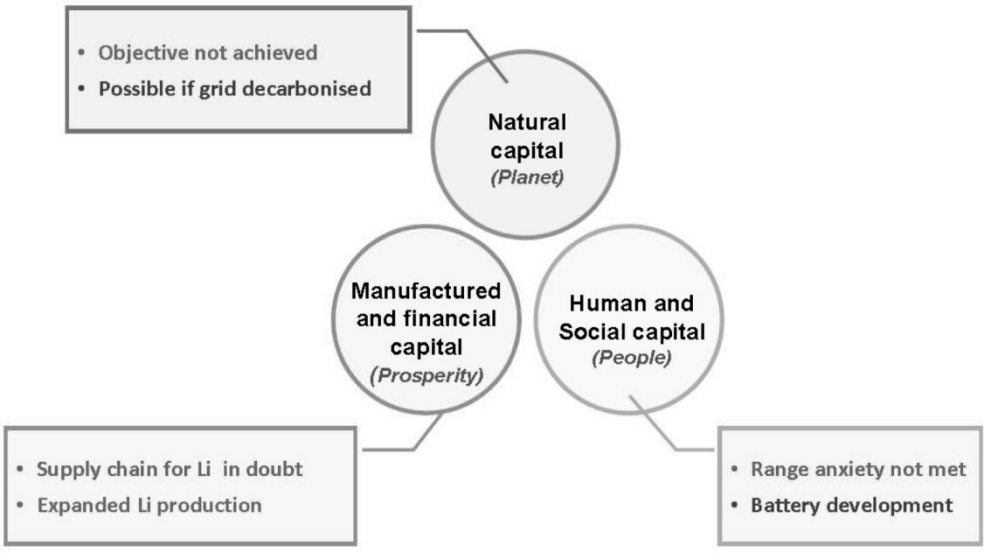

Figure 4. Assessment impacts [5]

Planet – the prime objective will not be met without grid decarbonized.

Prosperity – now is inadequate infrastructure for the production and recycling of Lithium.

People – their expectations of range anxiety are not currently met.

Step 5: Reflection
The issue of electric vehicles can be seen in the short-term (7 years), in this case, the electric car are not sustainable. In long-term (25 years), it is necessary to establish the infrastructure. Alternative strategy (for sustainability) is rethink car use.

5. Conclusion

Designers should not think about the design of the product only from a technical point of view, but in a broader context, as indicated in this contribution.

6. Acknowledgement

This paper was supported by the Project SGS-2013-050 "Complex support of design engineering of technical products to improve their properties and competitiveness II."

7. References

[1] ASHBY, M.: *Materials and the Environment: Eco-informed Material Choice.* 2nd ed. Elsevier/Butterworth–Heinemann, Boston, 2013.
[2] *CES EduPack software.* Granta Design Limiting, Cambridge, UK, 2012. (www.grantadesign.com)
[3] *Udržitelnýrozvoj* [online]. 13. 4. 2014. 2014 [cit. 2014-06-08]. Dostupnéz: http:// cs.wiki pedia.org/wiki/Trvale_udr%C5%BEiteln%C3%BD_rozvoj.
[4] ČSN 01 0391. *Systém Management Společenské Odpovědnosti Organizací – Požadavky.* Úřad pro technickou normalizaci, metrologii a státní zkušebnictví, Praha, 2013.
[5] ASHBY, M.: *Analysing Sustainable Developments and the CES EduPack Sustainability Database.* Webinar, Cambridge, 2014.
[6] TAKÁCS, A.: Generating Concepts with the Help of Green Tips. *Design of Machines and Structures*, Vol. 4, No. 2, 2014, Miskolc University Press, Miskolc.

Design of Machines and Structures, Vol. 5, No. 1 (2015) pp. 53–57.

OVERVIEW OF ANALYSIS METHODS OF ROLLING ELEMENT BEARINGS

DÁNIEL TÓTH–ATTILA SZILÁGYI–GYÖRGY TAKÁCS

University of Miskolc, Department of Machine Tools
3515, Miskolc-Egyetemváros
toth.daniel@uni-miskolc.hu; szilagyi.attila@uni-miskolc.hu;
takacs.gyorgy@uni-miskolc.hu

Abstract: In many cases, rolling element bearing defect is attributed to be one of the main causes of breakdown in devices. So that impede troubles, continuous condition monitoring is highly recommended. The following paper deals with several analysis techniques of rolling element bearings.

Keywords: *condition monitoring, rolling element bearing, signal processing*

1. Introduction

Permanent monitoring of machinery has been considered to be an essential and integral part of any modern manufacturing facility [1]. Device monitoring implies periodic or sequential collection and interpretation of data relating to the condition of hazardous components.

Rolling element bearings are important components of most machinery and their operating circumstances influence directly the operation of the entire machinery. Fault detection supports to determine the location of the fault so that corrective activity can be taken and maintenance work can be planned accordingly [2].

2. Rolling element bearing components

Bearing geometry is a crucial factor for identify bearing defects, because for example the geometry of ball bearings specifies the dynamics of the bearing components and their vibration attribute [3].

Generally, a rolling element bearing comprises two rings with a set of elements running in the tracks among the rings. Almost all of them feature cages. The cages decrease wear, friction, provides equivalent spacing and prevents the elements from friction against each other. Rings and rolling elements material are typically made of low-alloyed, through hardening chromium steel. As lubricant supply is burdensome with rolling element bearing geometry, bearings are frequently packed with thick greases and then sealed so that the bearing operates under lubrication. The standard types of a rolling element comprise ball, tapered roller, cylindrical roller, barrel roller and needle roller [4].

3. Condition monitoring methods

Condition monitoring is one possibility of a predictive maintenance program. The information collected can be used to specify machinery problems and corrective actions can then be implemented.

Several methods are used for the perception of bearing condition monitoring. The techniques are broadly classified as acoustic measurements, noise analysis, temperature monitoring, wear debris detection, vibration analysis etc.

3.1. Acoustic measurement

Acoustic measurement is receiving increasing attention in condition monitoring of rolling element bearings. The most effectual acoustic-based bearing health monitoring is acoustic emission. This is a transient impulse generated by the rapid release of strain energy in solid material under thermal or mechanical stress. The perception of cracks is the main application of acoustic emission. Thus, this method can be used as a device for condition monitoring of bearing defects and shaft cracks. The acoustic emission is not influenced or disturbed by other mechanical noise, and defects in rotating machinery, such as misalignment and unbalance, which cannot be eliminated lightly and entirely. So the acoustic emission based methods are superior in certain areas, especially for initial fault detection in rolling element bearings [5]. The acoustic emission process is capable of detecting defects forming deep inside the material, even before it would propagate out to the surface [6]. The measurement of a machine's sound can also be employed for diagnosing defects in bearings. Usually, the precision of these methods depends on sound pressure and sound intensity data [3].

The most frequently used acoustic emission parameters are energy, counts, rms, amplitude and duration time. The representation of acoustic emission parameters illustrated in Figure 1.

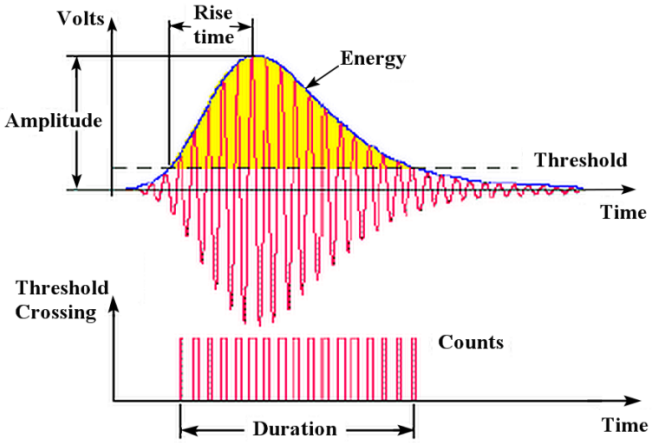

Figure 1. Acoustic emission parameters [7]

3.2. Noise analysis

Even though the most advanced manufacturing technology is used, sound still befall naturally in rolling element bearings. Since the noise emitted by bearings is composed of all types of faults developed during the working time of the bearings and the manufacturing process, the effective values of certain noise quantities enable quick and accurate examination [8].

Race noise is enough elementary sound in rolling bearings. It is a smooth and continuous sound. The magnitude of this noise is used to assess bearing quality. The frequency of this sound does not modify even if rotational speed changes, as shown in Figure 2.

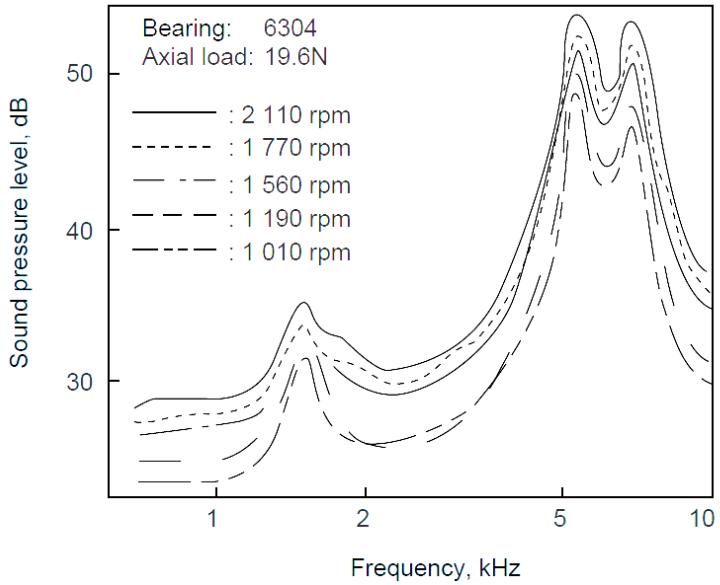

Figure 2. The impact of rotation speed on race noise [8]

Race noise is considered to be caused by configuration mistake, which happens even though the most advanced machining technology is used to process the surfaces of the raceways and rolling elements of a bearing. There are no particular countermeasures to eliminate the race noise entirely, but it can be minimized by perfecting the overall quality and precision of bearings [8].

Squeal noise is a metallic noise that can be rather loud in certain cases. This noise tends to occur with comparatively large bearings used under a radial load. It occurs usually in cylindrical roller bearings, but can also occur in ball bearings [8].

Click noise is generated merely at low speeds and cease when speed exceeds a concrete level. It is the collisions among the rolling elements and the cage and/or inner ring which cause click noise. It tends to occur more frequently in comparatively large bearings under radial loads [8].

Cage noise is attributed to the rotating cage colliding with raceway rings or rolling elements. Since there is clearance among the cage and both the raceway rings and rolling elements, it is cumbersome to fully eliminate cage noise. Nevertheless, it could be reduced to some extent by reducing the mounting mistake [8].

When a defect such as a rust or dent exists on a finished raceway surface of a rolling bearing, then a pulsating, machine-gun-like noise is created if the bearing rotates. In this case the level of the entire frequency spectrum rises [8].

Noise analysis technique can be implemented in conjunction with widely used signature analysis methods like cepstrum analysis, time domain statistics and spectrum analysis to meliorate the overall diagnostic and detection ability of these conventional methods in the presence of severe noise [9].

3.3. Temperature monitoring

Heat emission is a phenomenon that accompanies nearly each dynamic activity. Rolling element bearing distributed defects generate excessive heat in the rotating components. Rolling bearing manufacturers have long been aware of the connection of heat to bearing life and have designed formulas to precisely calculate safe operating temperatures. The outcomes indicate a temperature band in which both lubricants and bearings will operate at top performance with the least stress. As soon as outside the ideal temperature range, they will degrade at an accelerated rate [10].

Figure 3 shows the temperature range of a typical rolling element bearing. The red zone represents the critical section, the yellow zone symbolizes the decreasing lubricant and bearing life, the green zone expresses the sweet spot for bearing and lubrication temperature [10].

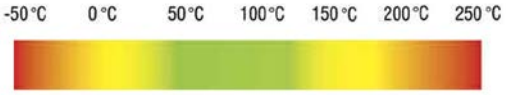

Figure 3. Thermal ranges of rolling element bearings [10]

Exist different temperature bands for distinct combinations of bearing and lubricant, but they will have the identical general trend regarding the optimal operating temperature and its effect on accelerated wear and failure.

Thermal imaging empowers real-time temperature monitoring and localization of temperature increases. Nevertheless, it allows a spatial visualization of heat propagation in monitored areas [11].

3.4. Wear Debris Analysis

The wear progress of a given machine is generally the result of many different, simultaneous wear mechanisms, each of which has its own way of affecting to the machine's operating environment and the changes that occur in it. When the poor operating conditions persist, the wear could either inflict parts of the machine to break or disturb the machine's operation. To allow detection at an untimely phase and control of the wear process, the amount, size, and appearance of wear debris particles in the machine's lubricating oil must be monitored [12].

In this technique, the presence of metallic particles in the lubricant is detected by sensitive sensors. Additionally, the spectrographic analysis of the dissimilar metallic elements in the lubricant could facilitate the location of the defect [3].

3.5. Vibration analysis

Vibration monitoring is a helpful tool in the maintenance. As the anomalous vibration of rotary machines is the first sensory effect of rotary component fault, vibration analysis is extensively employed in the industry. Vibration analysis could be applied for the diagnosis of every type of faults even distributed or localized. Among other things the vibration measurement methods benefits are accurate results, low-cost sensors and specific information [3].

Vibration analysis techniques are Fourier-transform, artificial neural networks, fuzzy logic systems, Wavelet-transform, Wigner–Ville distribution, singular spectrum analysis and so on.

4. Conclusion

Several diverse methods have been evolved for monitoring and diagnosis of rolling element bearings in the past decades. Vibration based methods are well established for the condition monitoring of rolling element bearings, although they are not so effectual in detecting early defects in the bearing. Acoustic emission is receiving increasing attention as a complementary method for condition monitoring of bearings as acoustic emission is enough sensitive to incipient defects. Temperature monitoring of bearing is a quick method for fault perception in rotary machines.

5. Acknowledgement

This research was carried out as part of the TÁMOP-4.2.1.B-10/2/KONV-2010-0001 project with support by the European Union, co-financed by the European Social Fund, in the framework of the Centre of Excellence of Mechatronics and Logistics at the University of Miskolc.

6. References

[1] PATEL, J.–PATEL, V.–PATEL, A.: Fault Diagnostics of Rolling Bearing Based on Improve Time and Frequency Domain Features Using Artificial Neural Networks. *IJSRD*, Vol. 1, Issue 4, 2013.

[2] MISRA, A.–GUPTA, A.–UPADHYAY, S. H.–HARSHA, S. P.: Fault Diagnosis in a Low-Speed Rotating Shaft Using Vibration Signal Analysis. *MIT International Journal of Mechanical Engineering*, Vol. 2, No. 2, Aug 2012.

[3] KHARCHE, P. P.–KSHIRSAGAR, S. V.: Review of Fault Detection in Rolling Element Bearing. *IJIRAE*, Vol. 1, Issue 5, June 2014.

[4] *FAG Rolling Bearings Fundamentals.* Technical Information TI No. WL 43-1190 EA October 1999.

[5] HE, Yongyong–ZHANG, Xinming–FRISWELL, Michael I.: *Defect Diagnosis for Rolling Element Bearings Esing Aacoustic Eemission.* DOI: 10.1115/1.4000480.

[6] PATKÓ, Gy.–TAKÁCS, Gy.–DEMETER, P.–BARNA, B.–HEGEDŰS, Gy.–BARAK, A.–SIMON, G.–SZILÁGYI, A.: A Process for Establishing the Remanent Lifetime of Rolling Element Bearings. *XXIV. microCAD International Scientific Conference*, Miskolc-Egyetemváros, March 2010.

[7] OHTSU, Masayasu–UDDIN, Farid A. K. M.: Application of AE to Fracture Toughness and Crack Analysis by BEM in Concrete. *NDT.net*, Vol. 7, No., 9, September 2002.

[8] MOMONO, Masayasu–NODA, Banda: Sound and Vibration in Rolling Bearings. *Motion & Control,* No. 6, 1999.

[9] TIAN, X.–GU, F.–ZHEN, D.–TRAN, V. T.–BALL, A. D.: A Study on Transient Enhancement for Fault Diagnosis Based on an Active Noise Control System. In: *CM 2012 and MFPT 2012.* London.

[10] MATZAN, Eugene: Detecting Premature Bearing Failure. *Machinery Lubrication Magazine*, May 2007.

[11] SCHULZ, R.–VERSTOCKT, S.–VERMEIREN, J.–LOCCUFIER, M.–STOCKMAN, K.–HOECKE, S. Van: *Thermal Imaging for Monitoring Rolling Element Bearings.* QIRT, 2014.

[12] HALME, J. K.: Condition Monitoring of Oil Lubricated Ball Bearing Using Wear Debris and Vibration Analysis. *6th International Tribology Conference*, Perth, Western Australia, December 2002.

REVIEWING COMMITTEE

Secreteriat of the Vice-Rector for Research and International Relations,
University of Miskolc,
Responsible for the Publication: Prof. Dr. Tamás Kékesi
Published by the Miskolc University Press under leadership of Attila Szendi
Responsible for duplication: Erzsébet Pásztor
Editor: Dr. Ágnes Takács
Number of copies printed: 50
Put the Press in 2015
Number of permission: TNRT–2015–240–ME
HU ISSN 1785-6892 in print
HU ISSN 2064-7522 online

DESIGN OF MACHINES AND STRUCTURES
Volume 5, Number 1 (2015)

PUBLICATION OF THE UNIVERSITY OF MISKOLC– A SHORT HISTORY

The University of Miskolc (Hungary) was founded by the Empress Maria Teresia in Selmecbánya in 1735. After the first World War the university moved to Sopron, where in 1929, it started the series of university publications with the title Publications of the Mining and Metallurgical Division of the Hungarian Academy of Mining and Forestry Engineering (Volumes I-VI). From 1934 to 1947 the Institution became the Faculty of Mining, Metallurgical and Forestry Engineering of the József Nádor University of Technology and Economical Sciences at Sopron. The publications got the title Publications of the Mining and Metallurgical Engineering Division (Volumes VII-XVI). For the last volume before 1950 –due to a further change in the name of the Institution– Technical University, Faculties of Mining, Metallurgical and Forestry Engineering, Publications of the Mining and Metallurgical Division was the title. For some years after 1950 the Publications were temporarily suspended. After the foundation of the Mechanical Engineering Faculty in Miskolc in 1949 and the movement of the Sopron Mining and Metallurgical Faculties to Miskolc the Publications restarted with the general title Publications of the Technical University of Heavy Industry in 1955. Four new series –Series A (Mining), Series B (Metallurgy), Series C (Machinery) and Series D (Natural Sciences)– were founded in 1976. These came out both in foreign languages (English, German and Russian) and in Hungarian. In 1990, right after the foundation of some new faculties, the university was renamed to University of Miskolc. At the same time the structure of the Publications was reorganized so that it could follow the faculty structure. Accordingly three new series were established: Series E (Legal Sciences), Series F (Economical Sciences) and Series G (Humanities and Social Sciences). The latest series, the Series H (European Integration Studies) was founded in 2002. Design of Machines and Structures (**HU ISSN 1785-6892(Print), HU ISSN 2064-7522(Online)**) first published in 2003 as a part of the Series C.